DNA NANOTECHNOLOGY AS A TOOL TO STUDY MEMBRANE-BINDING EVENTS: THE ROLE OF RGD PEPTIDE SPATIAL ORGANIZATION ON αVβ3 INTEGRIN BINDING

by

Merlyn Vargas

A Thesis
Submitted to the
Graduate Faculty
of
George Mason University
in Partial Fulfillment of
The Requirements for the Degree
of
Master of Science
Bioengineering

Committee:

_____ Dr. Rémi Veneziano, Thesis Director

_____ Dr. Parag Chitnis, Committee Member

_____ Dr. Barney Bishop, Committee Member

_____ Dr. Michael Buschmann, Department Chair

_____ Dr. Kenneth S. Ball, Dean, Volgenau School of Engineering

Date:_____ Fall Semester 2020
George Mason University
Fairfax, VA

DNA Nanotechnology as a Tool to Study Membrane-Binding Events: The Role of RGD Peptide Spatial Organization on αvβ3 Integrin Binding

A thesis submitted in partial fulfillment of the requirements for the degree of Master of Science at George Mason University

By

Merlyn Vargas
Bachelor of Science
Universidad de Antioquia, 2016

Director: Rémi Veneziano, Assistant Professor
Department of Bioengineering

Fall Semester 2020
George Mason University
Fairfax, VA

Dedication

To the most understanding little boy, Jayden Levrini.

Acknowledgements

Just like everything in life, many things had to happen exactly the way they happened for me to be able to produce this work and present it here today. Thus, I am very grateful for every experience and every person that was part of this work or somehow made it possible.
First of all, I want to thank my advisor Dr. Rémi Veneziano for not only giving me the chance to join his lab but also offering me a research assistantship that made my studies much more affordable. I would like to thank him also for making my research journey an enjoyable experience. Research itself can be a challenging and frustrating path, but it was easier having an active and understanding mentor to guide me through it.
I would also like to thank my co-workers and other students in the lab that made possible some of the results in this work or indirectly helped. Joshua, for his great and effective contributions in the production and quantification of ssDNA scaffolds and the great brainstorming sessions. Ranya, for her assistance in some of my experiments and her help in the synthesis of scaffolds. Shrishti, for her good ideas for troubleshooting my experiments and the helpful discussions. Esra and Sean, for their willingness to help. It was very rewarding to work with sympathetic people that always kept a positive attitude.
Gratitude must go to my dissertation committee members, Dr. Parag Chitnis and Dr. Barney Bishop for their willingness to be part of this and their great feedback during my proposal preparation and presentation. I would like to thank Dr. Bishop also for allowing me to use his facilities for the fluorescence measurements.
So many thanks must also go out to the people that have done all the administrative work for me, Sharon Richards, Carol McHugh, Dr. Shani Ross and Claudia Borke. They were always incredibly attentive and helpful.
Last but not least, I am immensely grateful for the supporting roles that play a significant part of this. I would like to thank my husband Gino for all the encouragement and support; my parents-in-law Gerri and Michael for the unconditional help, this would not have been possible without all their assistance; my mamá (mother) and mamita (grandmother) for being my greatest motivation to pursue big things in life; and finally, my son Jayden who despite his young age was always considerate and patient.

Table of Contents

Page

List of Figures

Abstract

DNA NANOTECHNOLOGY AS A TOOL TO STUDY MEMBRANE-BINDING EVENTS: THE ROLE OF RGD PEPTIDE SPATIAL ORGANIZATION ON AVB3 INTEGRIN BINDING

Merlyn Vargas, MS

George Mason University, 2020

Dissertation Director: Dr. Rémi Veneziano

Receptor-mediated recognition, interaction and entry into cells are fundamental mechanisms in cell biology notably for the control of cell fate and behavior [1]. However, the role of specific spatial arrangements of biomolecules in the recognition and binding by receptors, as well as the kinetic parameters of these interactions for many biological mechanisms is still not yet fully understood. For example, while the RGD (arginine-glycine-aspartate) peptide is a highly conserved motifs present in numerous proteins of the extra cellular matrices (ECM) involved in cell adhesion and migration its exact mechanism of interaction with cell receptors is still not fully elucidated. RGD is the principal integrin-binding domain present within ECM proteins such as vitronectin, fibronectin and fibrinogen [2]. To date, extensive efforts have been made in using RGD nanopatterns to investigate the influence of RGD organization adhesion of various cells and the relevant

proliferation, migration, and differentiation behaviors [3]. However, the effect of the nanoscale organization of this peptide on the interaction with cell membrane receptors is scarce. This limited understanding is due to the lack of techniques that allow for nanoscale control of biomolecules organization and precise stoichiometry control. In 2014, Shaw and coworkers developed DNA origami nanostructures modified with ligands at well-defined positions to study the role of ligand nanoscale organization in membrane receptor-mediated signaling. They found that nanoscale spacing of ephrin-A5 regulates the invasiveness of breast cancer cells and demonstrated the usefulness of DNA origami to study this type of receptor/ligand interactions [4]. In a follow-up study Shaw et. al [5] (*Binding to nanopatterned antigens is dominated by the spatial tolerance of antibodies*) used DNA origami as a platform to understand the distance in which bivalent antigen could bind to a receptor. They found that the reach necessary for bivalent antigen binding for human IgG ranges from 3nm to 17 nm with strong binding affinity at 16 nm. More recently, Veneziano et. al used DNA origami nanoparticles to study the influence of number, spacing and nanoscale presentation of antigens on activation of B-cells. In their research it was found that B-cell signaling is maximized with five highly spaced antigens, and the activation increases as antigen spacing increases up to 30nm [6].

Hence, DNA origami appears a promising tool to study the impact of the nanoscale organization of biomolecules upon binding interactions with receptors [6]–[8]. Indeed, DNA is a highly programmable biomaterial with great structural predictability that can be used to build high-fidelity assemblies [9]–[11]. Moreover, DNA can be easily functionalized using classical chemistry or using single stranded DNA (ssDNA) overhangs

and complementary ssDNA strands conjugated to the biomolecule of interest. Hence, molecularly precise nanoscale patterns of biomolecules can be displayed on a DNA origami structure making it realistic to study integrin-peptide interactions at the nanoscale level [4], [12].

DNA origami-RGD peptide systems represent potential for helping elucidate the role of RGD and its organization in membrane binding interactions, more specifically αvβ3 integrin binding. Using multifunctional DNA origami nanoparticles, we explored spacing, and 1D *vs* 2D organization of RGD peptide to bind the αvβ3 integrin at the protein level. DNA origami-RGD peptide systems not only represent potential for helping elucidate the role of RGD and its organization in membrane binding interactions but also to assemble the new generation of nanocarriers for drug delivery and effective scaffold for cell-tissue engineering.

Background

1. DNA Nanotechnology

DNA molecules, or deoxyribonucleic acid, play an essential role in human life. It is a biomolecule that exists mostly within the nucleus of cells in all living organisms and it is the carrier of the genetic information. DNA molecules consists of a double helix formed by the hybridization of two antiparallel complementary single stranded DNA (ssDNA) molecules via Watson and Crick Base-pairing. During the hybridization process DNA bases specifically pair up with each other, adenine (A) with thymine (T) and cytosine (C) with guanine (G), to form units called base pairs. Indeed, ssDNA molecules can self-assemble in solution with a complementary strand to form stable double stranded DNA (dsDNA) molecules [13].

The high predictability of DNA hybridization bonds, the addressability enabled by sequence specificity, as well as the unique structural feature of the dsDNA molecules have been exploited in the recent years to create nanoobjects. Since 1982, when Nadrian C. Seeman presented the possibility to form DNA objects, lattices, and crystals [14], DNA has been used to assemble a large spectrum of 1-,2- and 3D lattices and discrete nanostructures with nanoscale predictability. More recently, Paul Rothemund developed

the DNA origami technique that enables precise assembly of discrete, monodisperse and pure DNA-NPs in a one-pot reaction paving the way to the broad use of DNA origami in bioengineering and biomedical applications [10].

Besides the high structural predictability of DNA, there are many other properties that make this polymer a great scaffold material for biomedical applications. DNA nanostructures are fairly easy to functionalize. Using various conjugation techniques, such as click chemistry and ssDNA overhangs precisely located on the nanostructures, it is possible to link other functional and biological molecules to DNA or DNA nanostructures in very specific locations, orientation, and patterns [12]. Furthermore, DNA structures are biocompatible and biodegradable, in fact, they can be easily modified with biomolecules such as proteins or peptides to potentiate their biocompatibility [12], [15]–[17].

The unique properties of DNA nanostructures contribute to its importance in the design and development of materials and nanodevices with a wide range of applications [9]. In nanomedicine for instance, areas such as drug delivery, biosensing and tissue engineering are already incorporating DNA nanotechnology [18]–[21]. However, this technology still has few challenges to overcome, especially in scaling-up the synthesis process. The restriction in scaffold size and availability reduces our ability to create structures larger than a couple of hundred nanometers and the limitation in scaffold availability for large-scale production of nanoparticles has been limiting its use. Moreover, there is very few techniques available to produce modified scaffold that will reduce the cost of DNA origami synthesis and functionalization. In this thesis, we are presenting few innovative solutions that can help toward achieving these goals.

1.1. DNA Origami

DNA nanotechnology has gone through massive structural development since it has started in the 1980's. Early attempts to use DNA molecules to construct specific architectures from single branch points were unsuccessful [9]. The flexibility of DNA building blocks with a single junction point did not enable the creation of defect-free higher order structures. The introduction of multiple-crossover motifs overcame this limitation and provided the rigidity necessary for the assembly of larger objects. Especially, the double crossover tile, proposed in 1993 [22], [23] and shown in **Figure 1**, has become the motif of preference in DNA nanotechnology. As previously mentioned, DNA origami was first presented by Rothemund in 2006 [10]. In brief, DNA origami structures are assembled with a long ssDNA scaffold which is designed to fold into desired shapes held together by multiple complementary staple strands that bind to complementary regions of the scaffold [24]. Recently, researchers have implemented top-down techniques that complement DNA origami with DX-tile architecture to design and assemble DNA nanoparticles with any desire geometry or shape offering full control over1-, 2-, and 3D structure and local sequence [11]

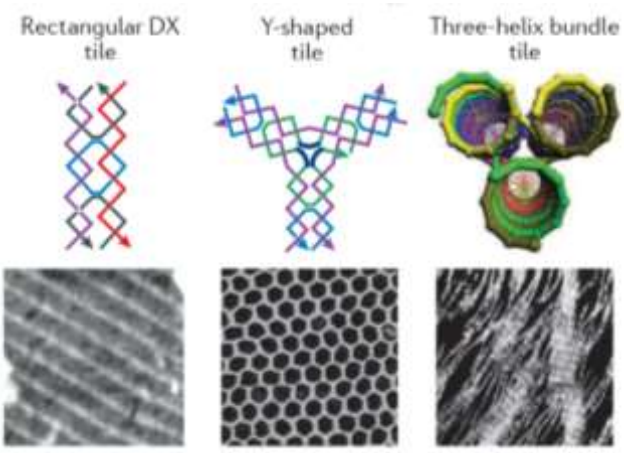

Figure 1.structural motifs in DNA nanotechnology. From Seeman (1993)

DNA origami is a technique that can be used to create nanostructures of high complexity while also providing a platform for precise arrangements and orientation of organic or

inorganic molecules, thereby extending their use to several biomedical applications [24]. Furthermore, DNA origami-based nanostructures have been used as molecular chips for label-free RNA detection [25], for triggered cargo release, immune stimulation, and as platforms for spatially-controlled enzyme cascades and analysis of dynamic molecular events [8], [24]. As its scaffold material, DNA origami nanoparticles have shown to be biocompatible, highly programmable and easy to conjugate [14].

1.1. DNA origami to study molecular interactions

Nanotechnology allow us to design and create objects at the nanoscale level. Before the rise of DNA nanotechnology, scientists had limited control over structure and organization of biomolecules at the nanoscale. Hence, DNA nanotechnology and particularly DNA origami has given us the opportunity to further understand interactions at the molecular level. Using this technology, one can assemble multiple organic or inorganic molecules while controlling their organization, orientation, and the exact location and spacing between them. Especially structural features such as stoichiometry and multivalency. The latter is characterized by simultaneous binding of multiple ligands on one biological entity to multiple receptors on another [26], [27]. As an example, this increase in the number of ligand-receptor engagement accounts for greater integrin avidity [28].

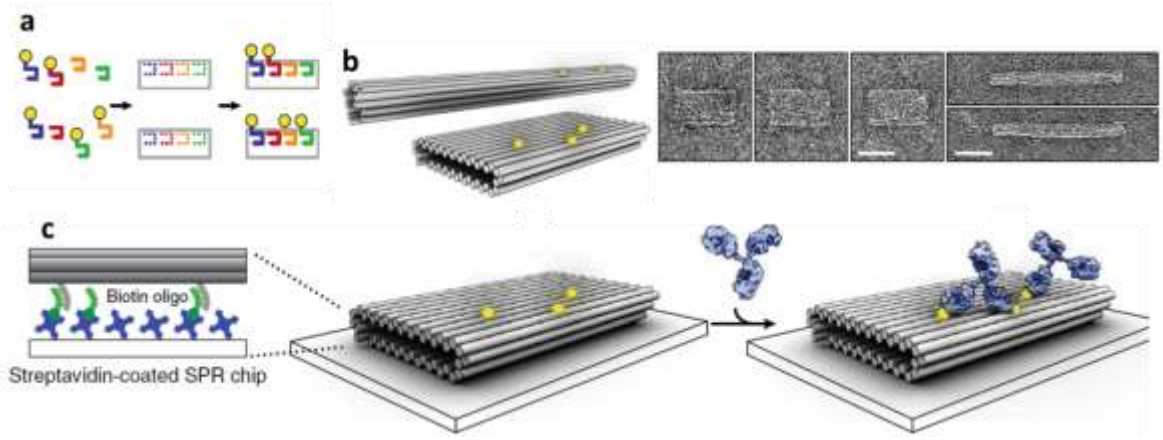

Figure 2. **a.** Antigen nanopatterns were fabricated using different combinations of antigen-decorated staple oligonucleotides (differently colored lines). **b.** 3D models using cylinders as a representation of double helices (left) and negative-stain transmission electron microscopy micrographs (right) of the DNA nanostructures used in the study. Scale bars, 40 nm. Two types of DNA nanostructures, an 18-helix rod and a 44-helix brick, were used to pattern the antigens. **c.** The antigen nanopatterns were immobilized onto a streptavidin-biotinylated oligonucleotide surface via oligonucleotide hybridization to sequences that protrude from the bottom face of the origami. Figure from reference Shaw et.al 2019.

Various approaches have been developed to engineer multivalent RGD-modified nanoparticles by linking multiple ligands together [29], [30] or presenting them in the surface of nanoparticles [31]. Such particles include liposomes, polymeric particles and other metallic particles. However, the inter-ligand distances in these particles are not well controlled and the stoichiometry cannot be controlled. The orthogonality of chemical modification is also a huge limitation with these particles that cannot be modified by more than 2-3 different type of molecules without compromising with the specific assembly. Recent progress in self-assembling DNA nanostructures with spatial and sequence addressability has made possible the study of this kind of phenomenon [26]. For instance, Shaw *et al*. introduced a method in which molecularly precise nanoscale patterns of

antigens are displayed using DNA origami and immobilized in a surface plasmon resonance set-up, as shown in **Figure 2.** Using antibodies with identical antigen-binding domains, they found that all the subclasses and isotypes of antibodies studied bind bi-valently to two antigens separated at distances ranging from 3 to 17 nm. The binding affinities of the antibodies change with the antigen distances, with a distinct preference for antigens separated by approximately 16 nm, and considerable differences in spatial tolerance exist between IgM and IgG and between low- and high-affinity antibodies due to the specific structures [5]. The importance of origami for single-molecule analysis was best illustrated in the label-free investigation of distance-dependent aptamer (short oligonucleotide)–protein binding by Rinker *et al* [26]. They designed DNA origami to display two different protein-binding aptamer sequences, with precise distance between them. In this studied they were able to find the distance at which the protein binds to this hetero-aptamers. Therefore, DNA origami appears as a promising tool to study the impact of the nanoscale organization of biomolecules upon binding interactions with receptors [7], [8].

2. RGD Peptide

The most extensively studied adhesive peptide in the biomaterials field is the RGD peptide, a tri-amino acid sequence, arginine-glycine-aspartate. RGD peptide is a widely used molecule to study cell adhesion and migration. It is highly effective at promoting the attachment of numerous cell types to a wide spectrum of materials [2], [32], [33]. It is the principal integrin-binding domain present within extracellular matrix (ECM) proteins such as vitronectin, fibronectin and fibrinogen [2]. The literature has extensively established that

RGD is the principal integrin-binding domain present within ECM proteins [2]. In addition, RGD peptides are well-known to bind preferentially to the αvβ3 integrin. An integrin that plays an important role in angiogenesis and that is highly expressed in tumoral endothelial cells as well as on various other tumor cells. RGD-based strategies are extremely promising for delivering anticancer drugs or contrast agents for cancer therapy and diagnosis [34], [35]

Cell responses to the synthetic ECM depend largely on multiple substrate features, such as its chemical composition, geometry, topographical features, and ligand organization. In 2009, Huang, J. *et al* [36] used a micelle nanolithography technique for making "ordered" and "disordered" Au-nanopatterns on glass surfaces decorated with RGD peptide to test the impact of the ligand distribution on the adhesion of tissue cells. Their findings along with other similar newer studies reveal that integrin clustering and such adhesion induced by RGD ligands is dependent on the local order of ligand arrangement [36], [37]. Furthermore, other studies have shown that RGD density influences not only cell internalization of biomimetic gold nanoparticles, but also human mesenchymal stem cells differentiation [38].

3. DNA origami to study RGD/ αvβ3 integrin interactions

Nanoscale organization of ligands has become an essential approach to study the clustering behavior of cell-surface receptors. Biomimetic substrates fabricated via different nanopatterning strategies have so far been applied to investigate specific integrins and cell types, but without precise multivalent control [39]. As mentioned in the previous section,

different strategies have been developed to create materials for the investigation of cell spreading and adhesion formation. These studies demonstrated that in order to establish stable focal adhesions and initiate integrin clusters, the examined cells require certain preferential spacing between single RGD peptides. However, these strategies have shown only partial application for multivalent investigations with single-molecule control. Repetitive patterns of ligands are crucial for certain cell responses and behavior. Still, an understanding of how integrins bind and dynamically interact with various spatial arrangements of adhesion molecules is lacking. Since, molecularly precise nanoscale patterns of biomolecules can be displayed on a DNA origami structure, It becomes realistic to study integrin-peptide interactions at this level [4], [12]. DNA origami-peptide systems could help us elucidate the nature of membrane binding interactions, but also represent potential devices for drug delivery and platforms for cell-tissue engineering.

In the present year, Hawkes and co-workers used DNA origami to surpass the limits of current approaches and fabricated nanoarrays to study different cell adhesion processes, with nanoscale spatial resolution and single-molecule control. They showed that DNA nanostructures conjugated to receptor ligands can be placed with high efficiency and precision onto surface. DNA nanostructures enabled the display of receptor ligands in a highly customizable manner, with modifiable parameters including ligand number, ligand spacing and stoichiometry. Their findings showed that different receptor types vary strongly in their clustering behavior; this demonstrates that previous findings from studies employing biomimetic arrays to study RGD/αvβ3 integrin interactions at the nanoscale are

not universally applicable. Therefore, further work is needed to investigate the nanoscale organization for different receptors and receptor combinations in detail [39].

Significance

Receptor-mediated recognition, interaction and entry into cells are important mechanisms in cell biology and in the control of cell fate and behavior [1]. However, the role of specific spatial arrangements of biomolecules in the recognition and binding by receptors, as well as the kinetic parameters of these interactions for many biological mechanisms is still not yet fully understood. For instance, mechanisms such as cell adhesion, migration and differentiation are fundamental biological mechanisms for which the role of nanoscale organization is still not clear. To date, extensive efforts have been made in using RGD nanopatterns to investigate specific adhesion of various cells and the relevant proliferation, migration, and differentiation behaviors [3]. Despite years of research, the effect of the nanoscale organization of RGD peptide on the interaction with cell membrane receptors is limited. Deeper knowledge of the binding dynamics of various densities and distribution of RGD peptide to integrin is crucial for a better understanding cell ECM interaction and cell behavior control by ECM. Our findings will have significant impact for basic understanding of the receptor ligand interaction and more broadly, for development of effective strategies for targeted drug delivery, vaccine development and tissue engineering among other biomedical applications that benefit from receptor-mediated mechanisms. This study will seek a better understanding of how the stoichiometry and precise nanoscale organization of RGD peptide on a DNA scaffold or nanostructure change the binding avidity from $\alpha v\beta 3$ protein.

Hypothesis

We hypothesized that the nanoscale organization of RGD peptide affects αvβ3 integrin receptor binding avidity. We planned to validate this hypothesis by comparing the dissociation constant (K_D) at small (5 nm) , medium (12nm) and large (18nm) peptide separation based on the head size of the integrin αvβ3 (8-12 nm) [37].

Multivalency enhances the binding strength of a ligand to its receptor and promotes receptor-mediated internalization of the bound entity [30]. To test this, we proposed to study the binding of nanostructures that presented the RGD peptide molecules in 2D at similar peptide spacings.

Specific aims

Aim 1. Synthesis of heavily modified scaffold for improved stability, molecules conjugation and imaging of DNA nanoparticles.

Asymmetric PCR (aPCR) was used to synthesize the DNA scaffold molecule, introducing multiple free amine (-NH_2) functional groups per molecule that was achieved with incorporation of modified bases to produce high functionality. The number of functional groups per molecule of DNA was characterized and quantified by attachment of Cy5-NHS (N-hydroxysuccinimide) reactive dye to the amine functional groups using NHS/NH_2 chemistry followed by purification by precipitation of the DNA. Finally, fluorescence spectroscopy was used to determine the number of dyes per molecule of DNA and then the number of free amine group. Using the same technique other molecules such as phosphorothioate group for DNA backbone modification were incorporated in the DNA for nucleic acid polymer stability in the presence of nucleases [36]

Aim 2. Investigation of the role of nanoscale organization of RGD peptide on αvβ3 integrin binding avidity.

One-dimensional DNA nanoparticles (80 nm long DNA origami nanorod) presenting RGD peptides (RGD-DNA-NP) with various inter-peptide spacing were investigated. Impact of linear peptide spacing on peptide-specific αvβ3 integrin binding was characterized to define critical minimum and maximum spacing needed for strong binding avidity.

Multivalent 2D spatial arrangements of RGD (on a quasi-plane on ~35 nm diameter pentagonal bipyramid DNA origami) were also evaluated for comparison with linear presentations of RGD to investigate the roles of multivalence and spatial presentation on αvβ3 integrin binding.

Chapter I. Synthesis of heavily modified scaffold for improved stability, molecules conjugation and imaging.

I. Introduction:

DNA origami is a technique that can be used to create nanostructures of high complexity while also providing a platform for precise arrangements and orientation of organic or inorganic molecules, thereby extending their use to several biomedical applications [24]. Furthermore, DNA origami-based nanostructures have been used as molecular sensors for label-free RNA detection [25], for controlled cargo release in drug delivery [41]–[43], immune stimulation [6], and as platforms for spatially-controlled enzyme cascades and analysis of dynamic molecular events [8], [24]. As its scaffold material, DNA origami nanoparticles have shown to be biocompatible, programmable and highly functionalizable [10], [11], [14], [15]. DNA origami structures are most often assembled with a long ssDNA scaffold, which is folded into desired shapes held together by multiple short complementary oligonucleotides (called staple strands) that bind to complementary regions of the scaffold [24]. M13mp18 bacteriophage's genome, a circular single stranded 7249 nucleotides (nts) long DNA, is the most used scaffold for DNA origami [44], [45]. Since the sizes of DNA structures are dependent of the length of the scaffold, the use of M13mp18 limits the size and properties of the DNA structures [46]. Various techniques have been used for the production of ssDNA scaffold, via chemical synthesis, enzymatic

amplification, and bacteria-based production [47], [48]. For instance, Polymeric chain reaction (PCR) is an enzymatic technique that uses a polymerase to amplify double stranded DNA from a DNA template. PCR can be used for the production of custom-size DNA molecules with sizes that can range from under a hundred and up to a few thousand base pair (bp). However, for the production of ssDNA from PCR, additional steps are necessary to purify the ssDNA strand of interest from the rest of the PCR products [47]. Some purification methodologies include biotin-streptavidin bead strand immobilization, where a biotin-modified primer is introduced in PCR amplification for subsequent biotin–streptavidin magnetic bead immobilization, dsDNA denaturation, and target ssDNA separation [49]–[51]. As an alternative method, preferential nuclease digestion of one of the strand of a duplex amplified by PCR is made possible by the incorporation of a phosphate group by one of the primer. This allows specific digestion of the phosphorylated strand and the obtention of the aimed ssDNA strand [52]–[55].

Alternatively, asymmetric polymerase chain reaction (aPCR) is a variation of the PCR technique that produces ssDNA directly. aPCR has been applied to synthesize custom-size ssDNA, ranging from several hundred to several thousand nucleotides in length [40]. However, aPCR technology for the production of DNA origami scaffold, still has few challenges to overcome in scaling up the process of synthesis, simplification of modifications and scaffold/nanoparticle stability. The restriction in scaffold size reduces our ability to create structures larger than a couple of hundred nanometers and the limitation in scaffold availability for large-scale production of nanoparticles has been

limiting its use. Moreover, there are very few techniques available to produce modified scaffold that will reduce the cost of DNA origami synthesis and functionalization.

Most applications of DNA origami require functionalized nanoparticles, and this is typically via chemical modifications of the staple strands used to fold the DNA origami. Importantly, PCR-based methods allow for the production of chemically functionalized ssDNA scaffolds with the introduction of modified nucleotides in the synthesis process [40], [56], [57]. Therefore, aPCR technology has the potential to simplify the production of heavily functionalized DNA origami, by the direct synthesis of modified scaffolds, when position of the functional groups is not a relevant factor. Modified nucleotide incorporation has been utilized in PCR and aPCR for the integration of reporter groups such as digoxigenin, biotin and fluorophores, as well as functional groups to provide increased thermal stability and nuclease resistance [40], [56], [58], [59]. For instance, Veneziano et. al demonstrated the capacity of aPCR to produce long fluorescent ssDNA scaffold (up to 10 Kb) with the incorporation of dye-labeled nucleotides and folded open wireframe DNA origami nanoparticles with such scaffolds [40]. However, the effect of modified nucleotides insertion on the yield of the PCR reaction has not been evaluated at this point, particularly for multiple modification, and very little is known on the effect of different percentages of modification on the properties of the scaffold. Therefore, in this study we present incorporation of various types of modified dNTPs in the aPCR reaction to produce functionalized scaffolds, the effect of the fraction of modified dNTP on the yield of ssDNA scaffold, and folding of functional nanoparticles with these scaffolds as illustrated in **Figure 3**.

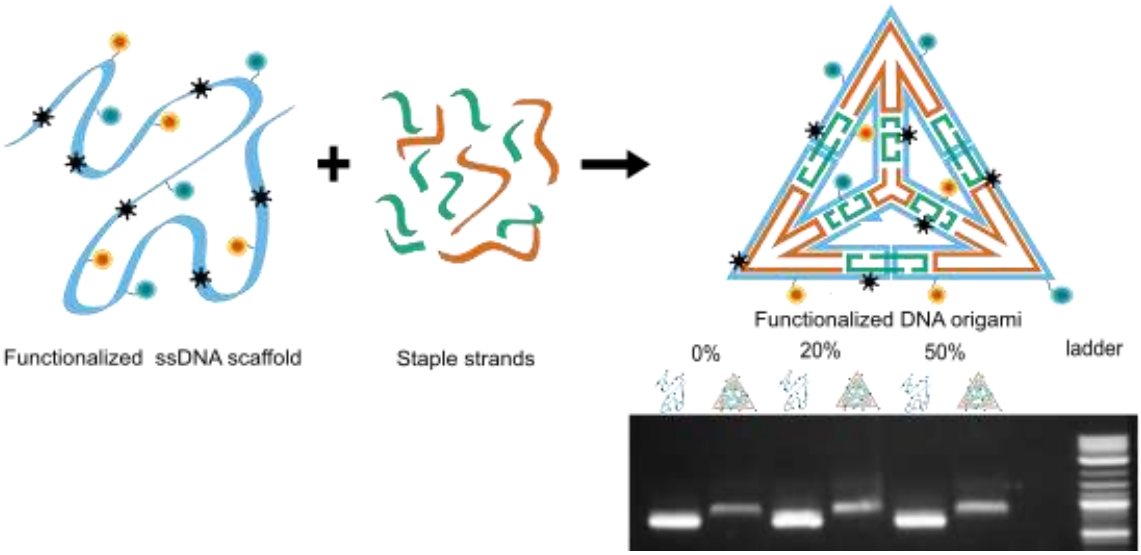

Figure 3. Folding of functionalized DNA origami using functionalized ssDNA scaffold and gel electrophoresis of functionalized scaffolds and their folded origami.

II. Materials and methods

Scaffold amplification using aPCR.

The ssDNA scaffolds were synthesized by aPCR as exemplified in **Figure 4** and described in [40]. Briefly we used the following amounts for a 50µl reaction tube: 1 µM of sense primer, 20 nM of antisense primer, 0.5µg/ml of M13mp18 ssDNA template, 200µM of deoxynucleotide triphosphates (dNTP), 1X HiFi PCR buffer, 2mM of magnesium sulfate ($MgSO_4$) and 1.25 U of AccuStart Taq DNA Polymerase HiFi (Quantabio). The aPCR was carried in a Bio-Rad T100 Thermal Cycler using the following program as follows: 94°C, 1 min for the initial denaturation; followed by 30 to 40 cycles of 94°C, 20 s; 55° to 59°C, 30 s; 68°C, 1 min per kilobase to amplify [11].

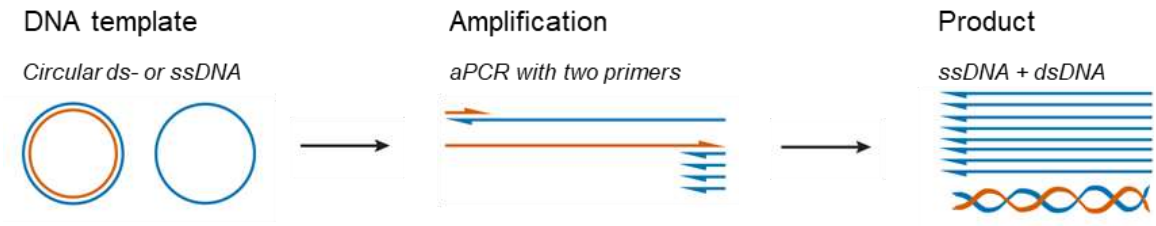

Figure 4. aPCR amplification adapted from reference (Bush et.al, 2020).

Agarose gel electrophoresis and ssDNA purification

Electrophoresis was used for the purification of ssDNA following aPCR reactions. The aPCR products were loaded in 1% low melt agarose gel made with Tris-acetate EDTA buffer and prestained with EtBr. A BioRad electrophoresis unit was used and the gel was run for 25 minutes under 100 V at room temperature. Gels images were taken with an Azure c150 gel imaging workstation and analyzed with Image J software to estimate the yield of ssDNA production. The ssDNA extractionwas done with a Zymoclean Gel DNA recovery kit. The gel band containing the ssDNA product was cut and removed from the rest of the gel using a single edge industrial razor blade. Then, 1 ml of agarose dissolving buffer, per each 300µl of PCR products, were added to the excised gel fragment and incubated at 50°C for 10 min or until the gel was completely dissolved. The melted agarose gel solution was added on to the spin column and centrifuged for 1 minute at 11,000xg. After it was completely loaded, it was washed with DNA wash buffer and the ssDNA was eluted from the column with 10 µL of water and centrifuged into a clean sample collection.

The concentration of the ssDNA collected samples was measured using a Nanodrop One microvolume UV-visible spectrophotometer (ThermoFisher).

Conjugation of Cy5 to NH_2 modified ssDNA

In a 1.5 ml sample tube, 20 pmol to 30 pmol of $(NH_2)_x$-DNA were mixed with Cy5-NHS ester in dimethylformamide (DMF) ensuring a 50X excess molar ration (considering 100% incorporation rate of modified dNTPs in the scaffold), about 30% v/v DMF and 20% v/v of buffer (100mM HEPES pH 8.2) in the final volume of reaction . If necessary, the volume of reaction was completed with Ultrapure DNA/RNA free water to a total of 100 µl and the tube was sealed and wrapped with aluminum foil, and left to agitate overnight in a rotisserie.

Purification of Cy5 conjugated ssDNA

After reaction between the amine modified scaffold with Cy5 NHS ester, the sample (around 20pmol or more ssDNA) was transferred to a conical 1.5 mL sample tube. Mixing well, sodium acetate solution (3M pH 5.2) and absolute ethanol (Isopropanol for small strands) at -20^{o}C were added to final percentage of 8% v/v and 70% v/v respectively in a total volume of approximately 300 µl. The tube was kept at -20^{o}C for at least 2 hours before it was centrifuged at 30,279g at 0^{o}C in a Sorvall ST 8 small benchtop centrifuge for 4 hours to form a ssDNA pellet, followed by removal of supernatant and two washes with ethanol at -20^{o}C and centrifugation for 15 minutes after each wash. After carefully discarding the supernatant to avoid the pellet disruption, the pellet was let to dry overnight and resuspended in water before further use and stored at -2^{0}C.

DNA origami folding and purification

The DNA origami folding was done in a one pot reaction following the protocol previously published by Veneziano et al [11]. Briefly, a 100k Amicon Ultra centrifugal filter was used for the purification and concentration of the DNA nanoparticles, where 300 to 400 ul of ~40 nM DNA nanoparticles were concentrated to a volume of around 70 ul with a recovery yield close to 70% for 6HB and 100% for PB.

Fluorescence spectroscopy

A Cytation 5 Cell Imaging Multi-Mode Reader (BioTek) was used in the fluorescence intensity detection mode with a fixed excitation at 590/20 nm and emission measured from 640/20 nm to 700 nm with 3 nm increments, from a read height of 7 mm with a Xenon flash light source at high lamp energy spectroscopy . Using free Cy5-PEG-NHS a standard curve was reproduced from 0 to 2,000nM for proper quantification of Cy5 in our samples.

III. Results and discussion:

Introducing functional groups in ssDNA scaffolds during aPCR amplification

Most applications of DNA origami require some degree of nanoparticle functionalization/conjugation. Certainly, this can be substantially facilitated by the integration of highly customizable functional groups in the ssDNA scaffold that allow for simplified chemistry, such as free amine groups. Additionally, stability of DNA origami in biological conditions is important for its adoption in the field of nanomedicine. In this project, the synthesis of functionalized ssDNA scaffolds of various sizes including 449 nts,

1616 nts (PB scaffold) and 1640 nts (6HB scaffold), was done with aPCR as described in the methods section, but introducing various functionalized dNTP mixtures. Amine-modified ssDNA scaffolds ($(NH_2)_X$-ssDNA) were synthesized using amine-modified deoxycytidine triphosphate (NH_2-dCTP) at various percentages in the dNTP mixture (0%, 10%, 20%, 50%, 75% and 100%). For alpha-thio-modified ssDNA(α-thio$_X$-ssDNA),

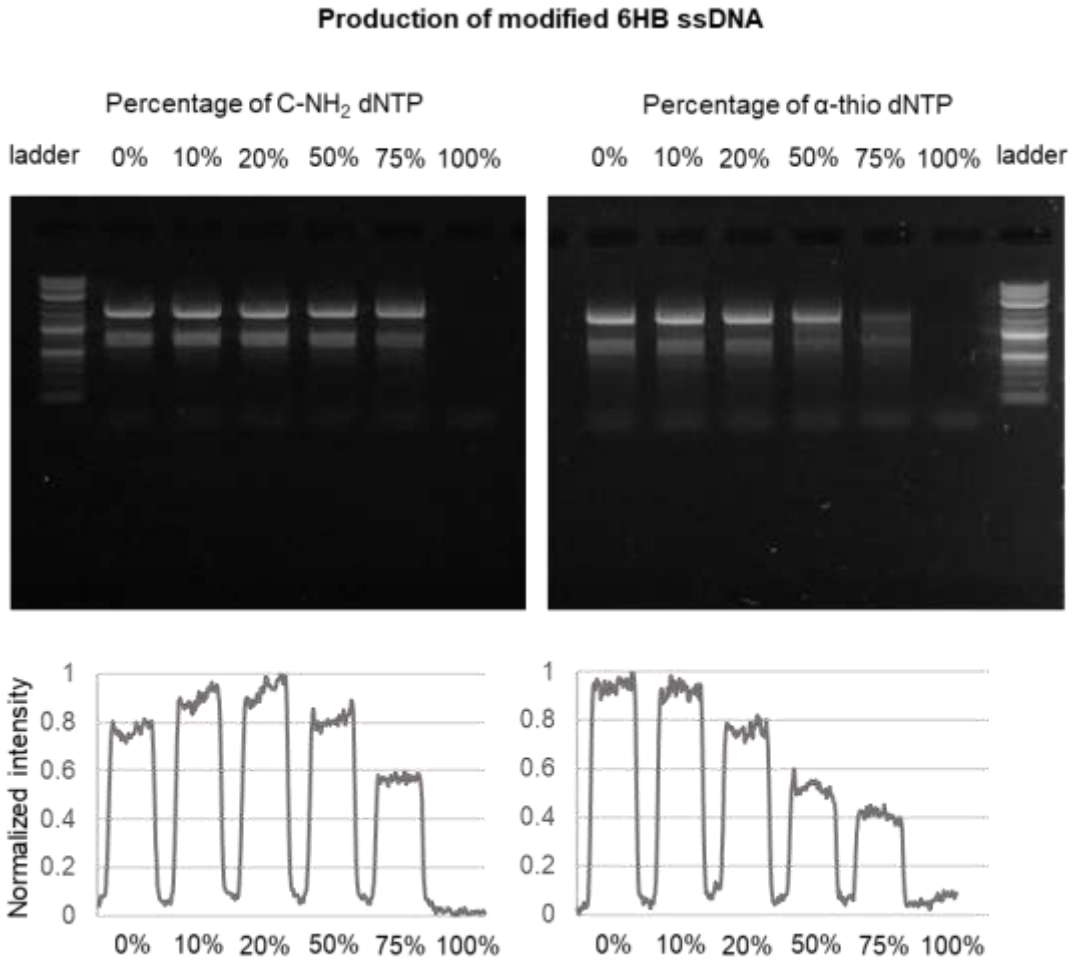

Figure 5. Image analysis of 1 % High melt agarose gel of 6HB scaffold produced with dNTP mixtures at various percentages of amine (left) and alpha-thiol (right).

alpha-thio dNTPs (alpha-thio deoxyadenosine triphosphate (dATP), alpha-thio deoxycytidine triphosphate (dCTP), alpha-thio deoxythymidine triphosphate (dTTP) and alpha-thio deoxyguanosine triphosphate (dGTP)) were used, along with non-modified dNTP to produce various percentages of modification as well (0%, 10%, 20%, 50%, 75% and 100%). Then, the scaffolds were purified from the rest of the products using gel electrophoresis and the DNA recovery kit as presented in the methods above. The ssDNA produced was quantified in two independent experiments using distinct replicates for each scaffold quantification. **Figure 5** presents the results observed from agarose gel electrophoresis of the 6HB scaffolds synthesized with various concentrations of amine-modified dCTP in the dNTPs mixture, also named as C-NH2 dNTP, and alpha-thio dNTPs (α-thio dNTP). With both types of modified dNTPs, amine and alpha-thio, the aPCR reaction led to a clear decrease in the amount of product as the percentage of modified dNTPs was increased, and finally no products were observed at 100% of modified dNTPs. The findings observed in gel analysis were confirmed with the actual quantification of the scaffolds and displayed in **Figure 6,** where a decrease of 40% to 50% of ssDNA yield was observed with 50% α-thio dNTP and 75% C-NH2 dNTP.

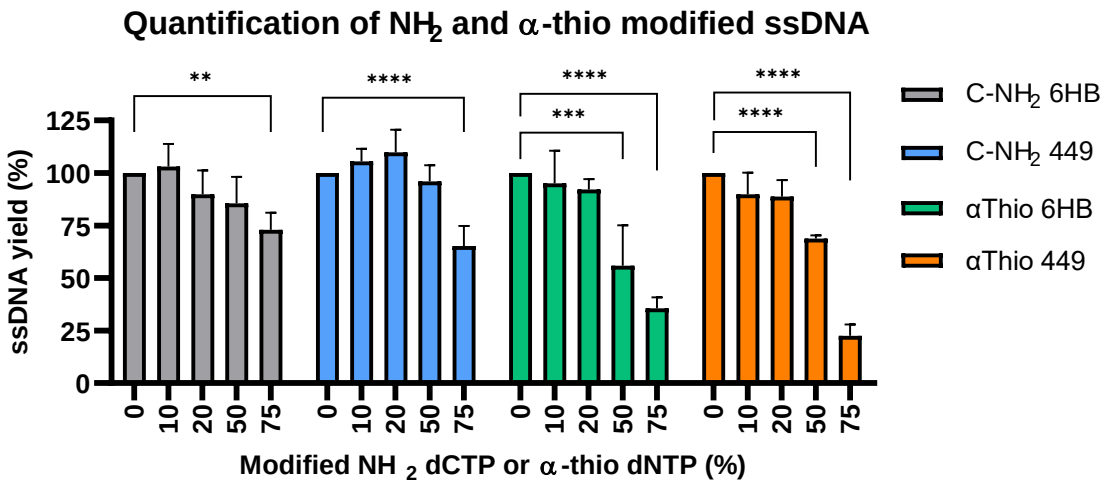

Figure 6. Quantification of scaffolds obtained with aPCR using dNTP mixtures at various percentages of amine modified C base and alpha-thio modified A,T,C and G bases. Error bars represent standard deviation of the mean (n = 4 replicates per group). P values are from a one-way ANOVA, (**P < 0.01, ***P < 0.001 and ****P < 0.0001).

The reduction of scaffold production yield is particularly important in the case of alpha-thio-modified scaffolds, with a decrease of almost 50% of the yield for 50% modified dNTP. In contrast, the amino-modified scaffolds were produced with no significant reduction of their yield with up to 50% modified dCTP. It is necessary to note that, we used the four modified bases for the α-thio vs only one base for the NH_2 modified dNTP which results in a larger number of base modified for the same percentage used. This overall higher amount of modify dNTPs explains the greater effect in yield of alpha-thio-modified scaffolds. Importantly, similar decrease in yield of aPCR products has been observed in

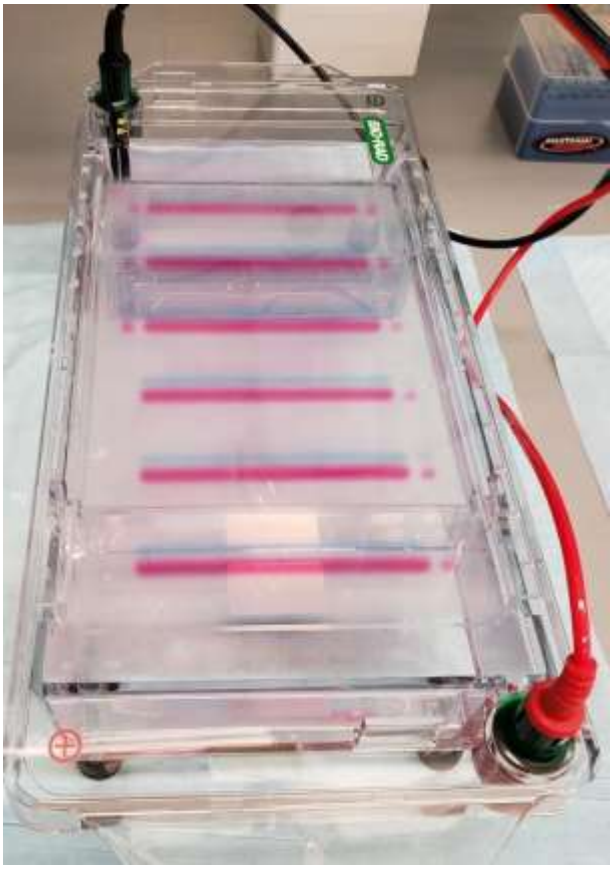

Figure 7. Scaling up ssDNA production from aPCR

gel analysis of modified scaffolds by Veneziano et al [40] and in double stranded DNA PCR products by Tasara et. al [59], but not real thorough quantification has been reported thus far. Additionally, production of scaffolds from aPCR was scaled-up to produce up to 260 pmol of ssDNA per 96-well plate. **Figure 7** displays the agarose gel electrophoresis to separate the aPCR products of one and a half 96-well plate in one gel.

Post synthesis scaffold functionalization, purification and DNA origami folding.

Thus far, we had produced amino-modified ssDNA (NH_2-ssDNA) that could allow for further and more customized functionalization of DNA origami scaffolds. To demonstrate this, we conjugated Cy5-NHS reactive dye to the free amine functional groups using NHS/NH_2 chemistry to obtain fluorescent Cy5x-ssDNA scaffolds and fluorescent DNA origami as a result. However, these scaffolds were now contaminated with excess Cy5-NHS and unwanted reaction buffers that could potentially affect the folding of origami with these scaffolds. In the literature, simple ssDNA purification technique to separate

small molecules from the Cy5x-ssDNA was not yet reported. Thus, we developed a precipitation method for purification of ssDNA by modifying similar approaches used in purification of dsDNA (see methods on page 19). As shown in **Figure 8**, the recovery efficiency of ssDNA with our methodology was in average 78%, which is higher than the 69.6% reported efficiency for dsDNA standard purification protocol [60]. Experimentally, better yields were observed at higher initial concentration of ssDNA.

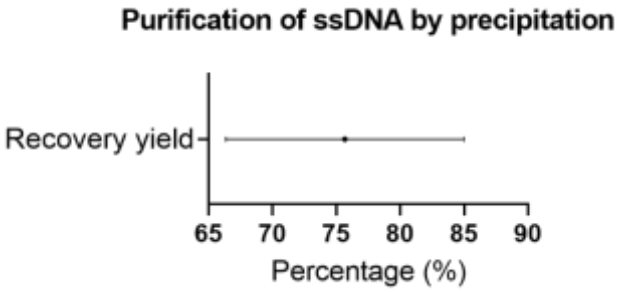

Figure 8. Recovery yield for purification of ssDNA by precipitation.

Consecutively, after producing the highly modified ssDNA scaffolds, it was necessary to test their ability to be used for folding of DNA origami structures. The Cy5x-ssDNA

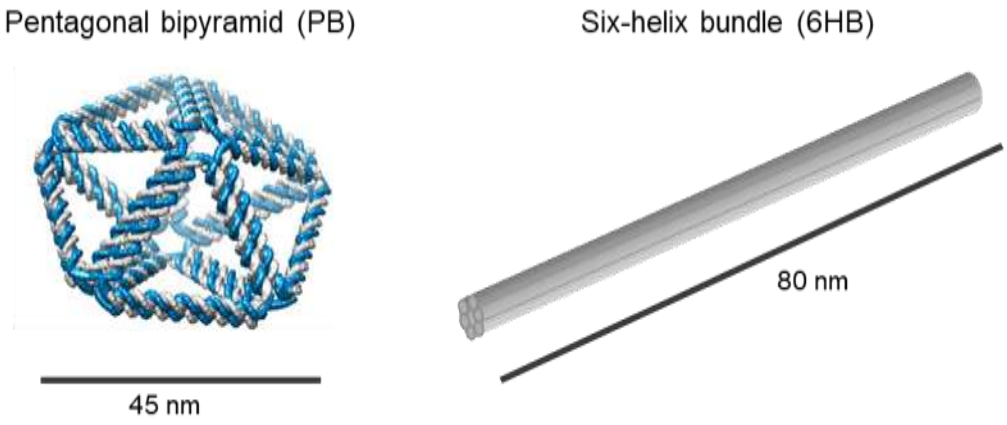

Figure 9. Illustration of the pentagonal bipyramid and six-helix bundle DNA nano structure

scaffolds produced from 20% and 50% amino-modified dNTPS were annealed with a set of regular staples to fold the six-helix bundle (6HB) and pentagonal bipyramid (PB) origami nanostructures (see **Figure 9**) following the DNA origami folding in the methods described in page 20. Both, corresponding scaffolds and folded origami, were run in 1.5% high melt agarose gel by electrophoresis, including a non-modified scaffold (0% amino-modified dNTPS) and its corresponding nanostructure. The results of the gel electrophoresis are shown in **Figure 3** and confirm the folding with a near 100% yield.

Efficiency of incorporation of NH_2-dCTP in the aPCR

Fluorescence spectroscopy was used to determine the number of dyes per Cy5x-ssDNA molecule, that could be used to estimate the number of free amine groups per molecule of ssDNA. This would help us to determine the rate of amino-modified dCTP incorporation in our scaffolds using aPCR.

One limitation of this method is the inherent limited efficiency of the NHS/NH2 reaction yield. By stating that number of Cy5 dyes equals number of initial NH_2 functional groups we are assuming a reaction yield percentage of 100% which is unlikely to happen for this type of reaction. However, using this strategy we are underestimating the number of NH2 functional groups knowing a least amount of them per DNA molecule. Indeed, for imaging purposes, we expect to get enough dye molecules to be able to track these nanoparticles for binding to cell membrane. Moreover, we could also incorporate click-chemistry group that have a higher efficiency of conjugation to mitigate this problem. We chose NHS/NH2 chemistry because the number of reactive molecules with NHS group surpasses the number of molecules available with click group.

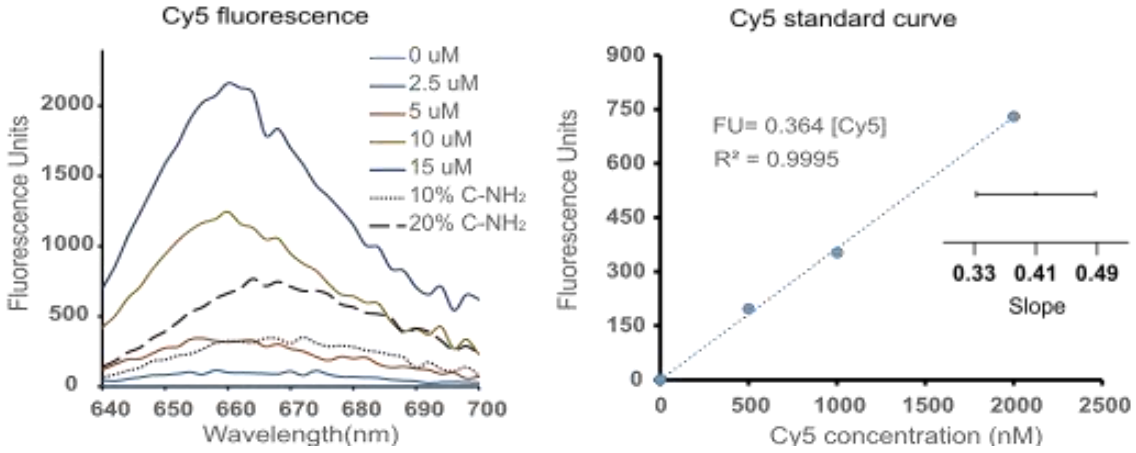

Figure 10. Cy5 fluorescence emission spectra (left) and standard curve (right). Inset: Distribution of the slope.

Figure 10 shows the fluorescence emission spectrum of Cy5 at various concentrations, including the Cy5x-ssDNA scaffold produced using 10% and 20% modified dCTP with a slight right shift in the spectrum that could be due to the influence of DNA on the spectrum of the bound dye [61]. We established a standard curve (**Figure 10** (right)) with free Cy5 dye and knowing the concentration of Cy5x-ssDNA in solution, we calculated the actual percentage of Cy5-modified-cytosine in a Cy5x-ssDNA molecule. The results are displayed in Error! Reference source not found.**.** Based on the fluorescence emission of ssDNA and purified origami, we estimated that the efficiency of incorporation of NH_2-dCTP in the aPCR is around 30% (20% modified dCTP lead to a modification rate of 6% and 10% modified dCTP lead to a modification rate of 3% Cy5-modified cytosine ssDNA scaffolds) (see Error! Reference source not found. (left)). As previously mentioned, and considering the efficiency of the NHS/NH_2 reaction to attach the Cy5 to the ssDNA scaffold, these numbers could be underestimating the real number of NH_2 group available

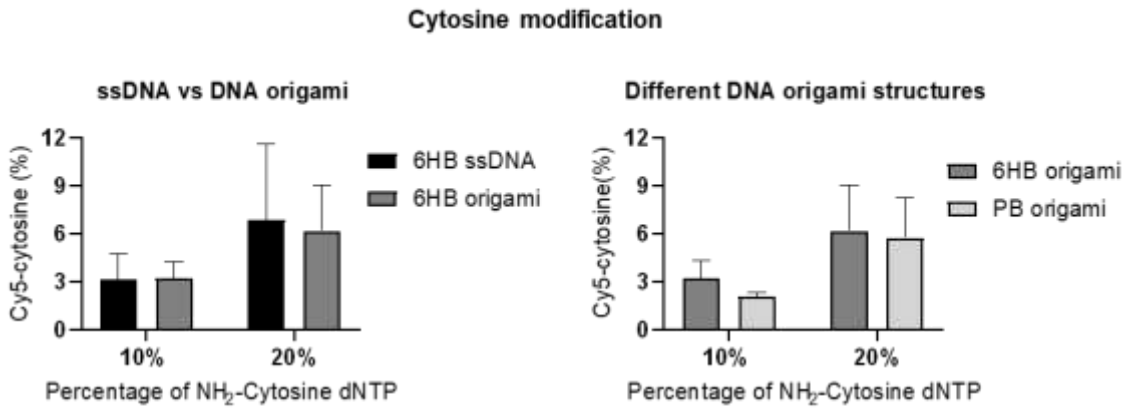

	Theoretical modification	#C/scaffold	#C modified	Actual modification
6HB ssDNA	10%	382	12	3.1%
	20%	382	26	6.8%
6HB origami	10%	382	12	3.1%
	20%	382	24	6.3%
PB origami	10%	337	7	2.1%
	20%	337	19	5.6%

Figure 11. Percentage of Cy5-cytosine in $Cy5_X$-ssDNA scaffolds and their corresponding origami nanostructure (left) and Percentage of Cy5-cytosine in two different DNA origami nanoparticles. The table in the bottom summarizes the number of C bases modified per DNA scaffold and origamis and their actual percentage of Cy5-cytosine modified .

that are incorporated with aPCR. For instance, Veneziano *et al*. used Cy5 modified dCTP directly in the aPCR to produce fluorescent ssDNA scaffolds that showed a 50% incorporation efficiency (5% modified dCTP produced 2.5% Cy5-modified cytosine ssDNA scaffold) [40]. However, our approach to the incorporation of functions in the ssDNA scaffold is easier, cheaper, highly customizable, and can be done on demand which reduce the risk of degradation of the dye.

IV. Conclusions:

Highly functional long (1,644 nts) and short (449 nts) ssDNA scaffolds with multiple free amine groups and phosphorothioate backbone were successfully synthesized using aPCR. These functional groups were randomly introduced into the scaffold utilizing modified dNTPs that are incorporated by the enzyme during the aPCR reaction. High ratios of NH_2-modified α-thio modified dNTPs can be used in the synthesis of both long and short scaffolds, with no significant impact in the PCR product yield, and the incorporation efficiency of amino-modified dCTP was calculated to be 30%.

Cy5 modified scaffolds were synthesized using a post-aPCR conjugation approach that reduces the cost of using Cy5 modified dNTPs directly in the aPCR. Additionally, a ssDNA purification method with up to 85% recovery yield was developed to purify such scaffolds to use for DNA origami folding. Importantly, fluorescent DNA origami nanoparticles with up to 24 Cy5 molecules conjugated were successfully synthesized/folded using our modified scaffolds.

V. Future work:

The effect of the incorporation of α-thio in the synthesis yield of ssDNA scaffolds was measured, but testing of the stability of these scaffolds is still lacking at this point. We plan to measure DNA nanoparticle stability using a Förster resonance energy transfer (fret) assay, where a pair of dyes are strategically position on the nanoparticles using staple design. Fret will be observed when nanoparticles are folded and dye are close to each other, but should decrease as the nanoparticles disintegrate in physiological medium.

The incorporation of multiple modifications in one reaction for the production of multifunctional scaffolds. We plan to incorporate other functional groups that allow easy chemistry and conjugation of biomolecules, as well small molecules to allow capturing of DNA origami nanoparticles, such as biotin and digoxigenin.

Our highly functional DNA origami nanoparticles can be tested as the platform or nanocarrier in cellular studies for targeting and cargo delivery of drugs, as well as for targeted cell imaging.

Chapter II. Investigation of the role of nanoscale organization of RGD peptide on αvβ3 integrin binding affinity.

I. Introduction:

As previously stated, DNA origami has been used to create nanostructures with high complexity, while also providing a platform for precise nanoscale arrangements and orientation of molecules. DNA origami has given us the opportunity to further understand interactions at the molecular level. Using this technology, we assembled multiple DNA nanoparticles to control the organization, orientation, and the exact location and spacing between the RGD peptide molecules. Techniques such as isothermal titration calorimetry (ITC), surface plasmon resonance (SPR) and bio-layer interferometry (BLI) are commonly used techniques to study protein interactions. However, SPR offer several advantages over BLI and ITC. Notably, it is a label-free interaction analysis technique with high throughput and small sample size that has been widely used for the investigation of RGD-αvβ3 interactions [29], [62]–[64]. SPR is an optical technique that use a gold coated glass (modified or not with specific molecules) sensor that allows for detection of refractive index changes at the surface of a sensor that enables measurement of biomolecules interactions. As shown in **Figure 12** , if a ligand is attached to the gold surface and an analyte is flowed over it, the interactions between the ligand and the analyte are detected

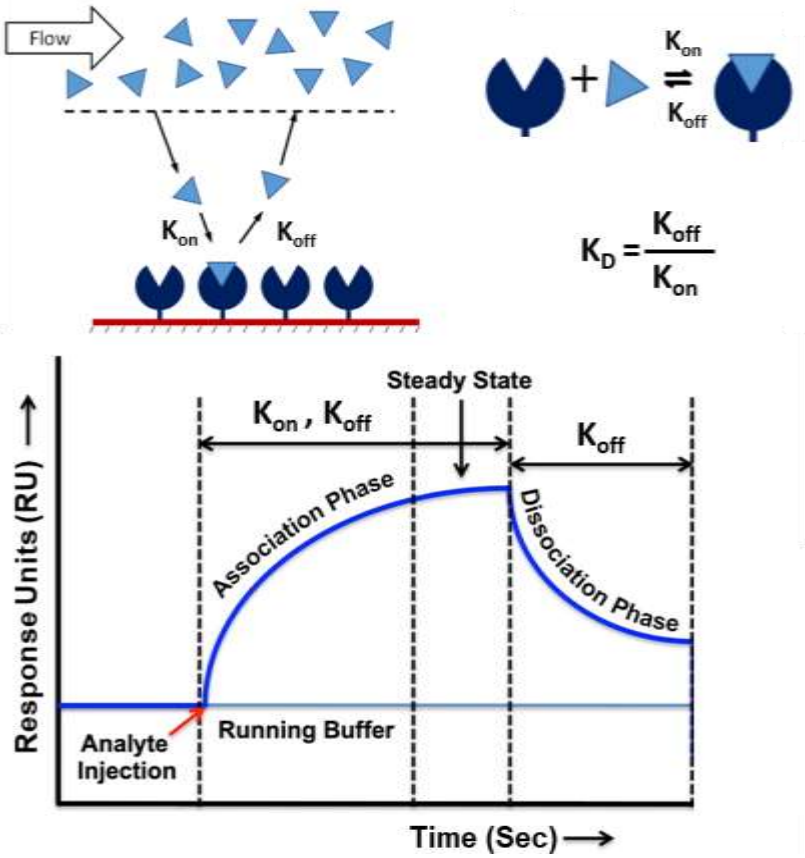

Figure 12. Surface plasmon resonance technique, adapted from reference *[70]* and Nicoya's website.

as changes in refractive index in the surface, and a binding curve is obtained. Thus, SPR can give us the kinetic information necessary to obtain the affinity constant (K_D) of nanopatterned RGD-DNA nanoparticles to the protein αvβ3. In this study, a DNA origami-SPR sensor platform was developed and implemented to study the impact of precise nanoscale organization of RGD peptide on the binding affinity from αvβ3 protein.

II. Materials and methods

RGD peptides were purchased from peptide international, RGD-azide or RGD-N_3 (RGD-3749-PI) and RGD-Biotin (PCI-3895-PI). The integrin αvβ3 was purchased from R&D systems (3050-AV-050).

Structure design

CadNano2 and Tiamat computer programs were used to design a six-helix bundle for the one-dimensional presentation of the RGD peptide and a pentagonal bipyramid for the two-dimensional presentation of RGD peptide. In this study, the position of the functional groups that will eventually hold the RGD peptide molecule on the DNA origami had to be controlled. We then carefully selected the staples to be modified with functional group in order to organize RGD peptides with nanoscale precision, as illustrated in **Figure 13.**

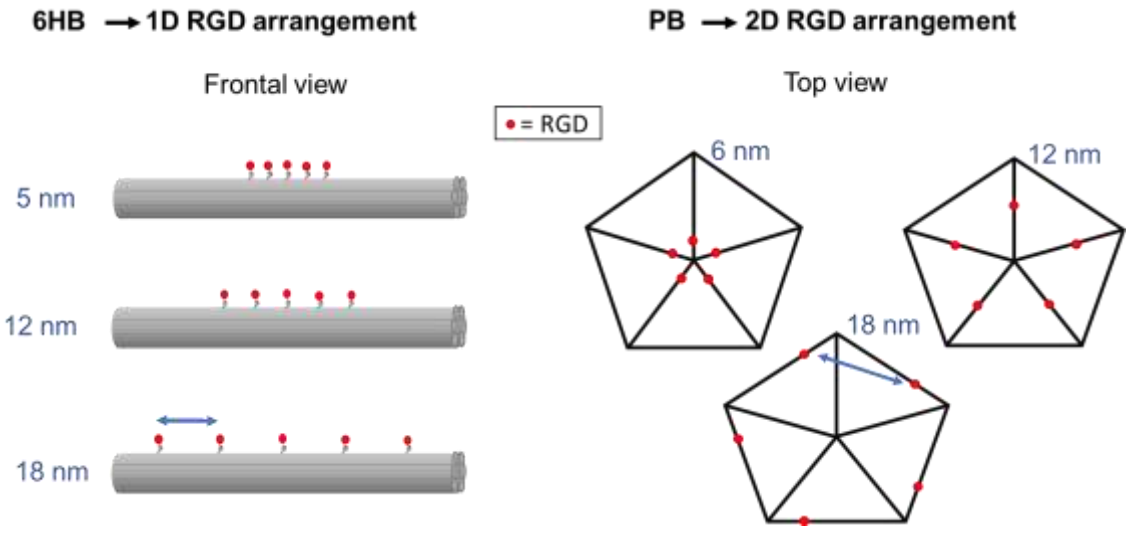

Figure 13. RGD-DNA origami structure design and RGD modification and controlled position

Five selected amino-modified oligonucleotides that were eventually going to be conjugated to RGD peptide, and five biotinylated oligonucleotides in the opposite side of the amino modified ones for attachment of the structures onto the SPR sensor, were introduced in the design.

Synthesis of ssDNA scaffolds

The synthesis was done using the aPCR method described in page 17.

Synthesis and purification of DBCO modified staples (DBCO-staples).

ssDNA-NH_2 + NHS-PEG_4-DBCO → ssDNA-DBCO

In a 1.5ml sample tube, 10 nmol of NH_2-staple were mixed with a DBCO containing linker (764019 Sigma-Aldrich, DBCO-PEG_4-NHS) in dimethylformamide (DMF) with a 50-fold greater concentration of DBCO linker, 30%-50% v/v DMF and 20% v/v of buffer (100mM HEPES pH 8.2) in the final volume of reaction. This tube was sealed and wrapped with aluminum foil, and left to agitate overnight in a rotisserie wheel.

Folding of DBCO-DNA-Biotin nanoparticles using modified staples

ssDNA (scaffold) + ssDNA-DBCO (staples) + ssDNA-Biotin (staples) → DBCO-DNA-NP

Using the folding method described in page 20, the DNA scaffold and modified staples (ssDNA-DBCO and ssDNA-Biotin) were hybridized to fold the nanostructures. The ssDNA-DBCO (staples) were at predetermined positions on the DNA nanostructure to control the location where the RGD molecules were to get conjugated. The DNA nanoparticles were purified and concentrated to around 150 nM using ultra-centrifugal filters with 100 kDa cut off to remove excess staples.

Functionalization of DNA staples/ DNA origami with RGD

Utilizing copper-free azide–alkyne cycloaddition [65], the DNA structures were combined with RGD-N_3 to obtain RGD conjugated structures:

DBCO-DNA-NP + RGD-N_3 → RGD-DNA NP

This reaction was carried in PBS 1X, the concentration of DNA nanoparticles was between 100 nM-110 nM (500 nM-550 nM of DBCO), and RGD-N_3 was added to a final concentration of 25 uM. The RGD modified DNA nanoparticles were characterized with agarose gel electrophoresis (AGE) to confirm the structures continued to be folded.

Preparation of biotin sensors for SPR

The SPR gold sensors were modified in two steps, first a self-assembled monolayer (SAM) of carboxylic functional groups was formed, then, from it a biotin surface was produced. The following material were used: non-functionalized SPR gold sensor chips were purchased from Nicoya, 11-Mercaptoundecanoic acid (674427 Sigma-Aldrich), N-(3-Dimethylaminopropyl)-N′-ethylcarbodiimide hydrochloride (EDC), N-Hydroxysuccinimide (NHS) and biotinylated bovine serum albumin (BSA-Biotin).

Initially, a solution of 11-Mercaptoundecanoic acid 2.2 mg/ml in absolute ethanol was prepared. The gold sensors were gently rinsed with water, then with 70% ethanol and finally dried with a clean air flow. Following, each gold sensor was placed in a clean and dry 10 ml beaker, that was filled with the 11-Mercaptoundecanoic acid solution, sealed and cover using parafilm and aluminum foil respectively and let to sit for 48 hours at room temperature.

The carboxylic SAM SPR sensor chips were thoroughly rinsed with 70% ethanol and water respectively, then dried with air. A mix of 50 µl of EDC 20 0mM and 50 µl of NHS 50 mM was prepared and quickly added on top of the gold on the sensor chip and let to react for 3 minutes. After the reaction is completed the excess solution was removed by tilting the sensor chip and 100 ul of BSA biotin at 0.5 mg/ml were quickly added on top of the gold, this was also let to sit for 3 minutes before it was rinsed with water and dry

SPR experiments

All the experiments were caried in a Nicoya Open SPR with running buffer (0.01 M HEPES pH 7.4, 0.15 M NaCl, 0.005% v/v Surfactant P20 supplemented to 1 mM $MgCl_2$ and 1mM $MnCl_2$). HCl 10 mM was injected at 150 µl/min to clean the surface of the biotin sensor before the streptavidin (1 mg/ml at 20 µl/min) was immobilized. The HCl injection was repeated to clean the streptavidin surface before injecting the biotinylated origami structures carrying the RGD patterns (prepared in the running buffer at 12 nM-15 nM) at 20 µl/min, followed by a 10 min buffer wash. Integrin αvβ3 was diluted in the running buffer to various concentrations, depending on its affinity towards RGD (0.5–53 nM). Injections were performed at 20 µl/min in increasing concentrations of the integrin with each concentration having a 3 to 5 min contact time and followed by a 10 min buffer wash.

SPR data analysis

TraceDrawer software was used to fit the SPR data to a 1:1 Langmuir binding model and calculate the K_{on} and K_{off} to obtain the K_D as illustrated in **Figure 12** . The values obtained in three independent SPR experiments for each RGD-DNA nanostructure, free RGD

(Positive control) and non-modified DNA nanostructures (negative control) were analyzed with repeated measures one-way ANOVA using GraphPad software.

III. Results and discussion:

Multiple steps including design of DNA origami, functionalization of staples, folding of multifunctional DNA origami and its RGD conjugation, were develop towards the construction of a DNA origami-SPR platform that allowed us to study the impact of precise nanoscale organization of RGD peptide on the binding affinity from αvβ3 protein. Firstly, as previously shown in **Figure 13,** one- and two-dimensional DNA origami structures were designed to control nanoscale organization of RGD molecules at determined positions that allowed us to control interpeptide distance (5nm, 12nm and 18nm for the one-dimensional DNA origami structure and 2 nm, 12 nm, and 18 nm for the two-dimensional one). As illustrate in **Figure 14**, five staples of each DNA origami underwent chemical reactions that would later allow us to incorporate the RGD peptide on to the structures.

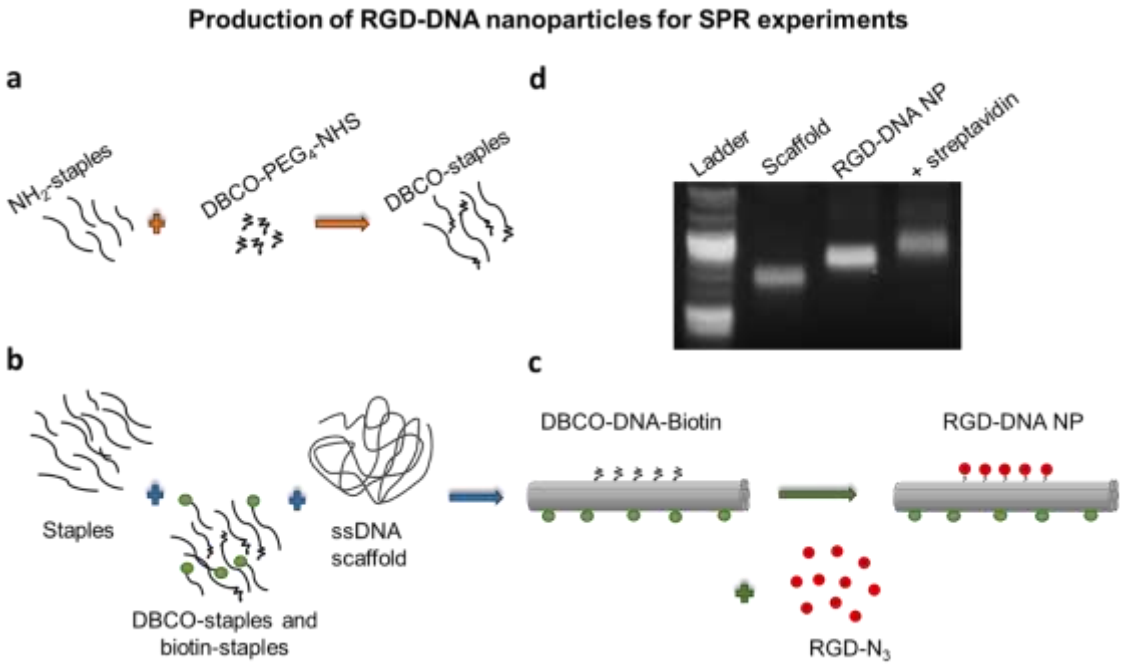

Figure 14. Process of production of RGD-DNA origami nanoparticles. **a.** Synthesis of DBCO modified staples (DBCO-staples). **b.** Folding of DBCO-DNA-Biotin nanoparticles using modified staples. **c.** Functionalization of DNA origami with RGD to produce RGD-DNA nanostructures. **d.** Picture of agarose gel of ssDNA scaffold, folded Biotin and RGD modified DNA origami nanoparticle (RGD-DNA NP) and RGD-DNA NP plus streptavidin to confirm the biotin in the structures can bind the streptavidin in the SPR experiments.

Modification of ssDNA staple strands with a Dibenzocyclooctyne (DBCO) linker

The staples that were going to be used for conjugation of the RGD on the DNA nanoparticles had an amino group on their 5' end. These amino-staples were let to react with a DBCO containing linker (NHS-PEG_4-DBCO) to obtain DBCO-modified staples, as it is illustrated in **Figure 14(a)** and described in page 34. To confirm the efficiency of the reaction, it was followed by copper-free azide–alkyne cycloaddition with RGD-N_3 to the DBCO-modified staples to obtain RGD-modified staples and validated with polyacrylamide gel electrophoresis (PAGE). However, initially this strategy was not very

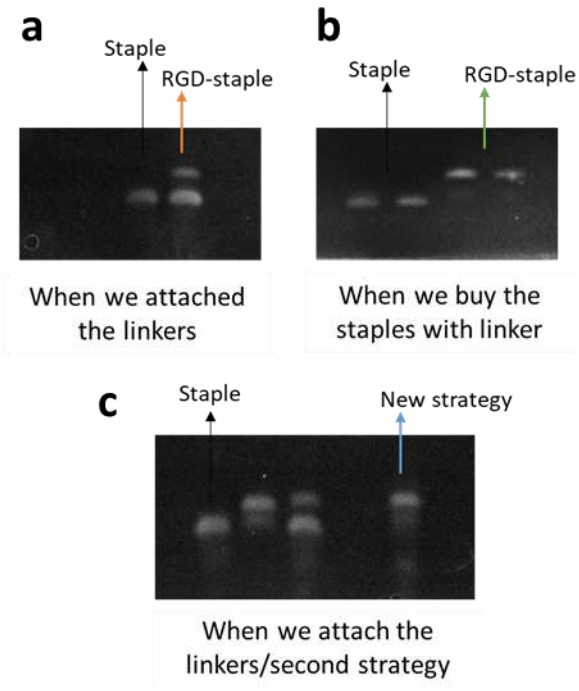

Figure 15. The conjugation of the ssDNA staples with RGD is highly limited by the yield of the NH_2/NHS reaction. **a.** shows the low conjugation yield obtain without two step reaction. **b.** the results of conjugation using a DBCO- modified linker showed much greater yield than our strategy. **c.** The yield of our RGD conjugation is highly improved with the increment of organic solvent in the first step reaction (NH_2/NHS).

efficient and a large fraction of the staples were not being conjugated to RGD as it can be seen in a PAGE gel in **Figure 15(a).** Knowing the high efficiency yields that can be achieved with copper-free azide–alkyne cycloaddition, it was very unlikely that this reaction was the problem. Thus, suspecting the NH_2/NHS reaction was the issue, ssDNA staple already conjugated to a DBCO linker (commercial DBCO-conjugated staple) were bought and let to react with the RGD-N_3 in the same way it was done before. **Figure 15(b)** shows that most of the DNA was successfully conjugated to the RGD. These results confirmed that some refining needed to be done to the NH_2/NHS reaction to attach the DBCO with greater yield. Consecutively, we found in the literature the same reaction performed with higher concentration of organic solvent to improve the solubility of the NHS-PEG_4-DBCO linker. After trying this new strategy for the NH_2/NHS reaction with 30-50% dimethylformamide in the buffer, greater yields of functionalization were obtained. These results are shown in **Figure 15(c)**, where we demonstrate that our strategy yield comparable results with the results from the commercial DBCO-conjugated staple.

Efficient production of RGD conjugated DNA nanoparticle

As illustrated in **Figure 14 (b),** after successfully producing DBCO-conjugated staples, the DNA origami structures that contained biotin groups and DBCO linkers as a result (DBCO-DNA-Biotin) were folded. Consecutively, RGD-N_3 was conjugated to the DBCO-DNA-Biotin nanoparticles following the protocol on page 35 of the methods section to produce RGD-DNA nanoparticles (see illustration of this on **Figure 14(c)**. Based on the shift of the bands on the gel picture in **Figure 14(d)**, the folding of the RGD-DNA nanoparticles was effectively confirmed. Also, the presence of biotin, that would later allow the attachment of these structures on the surface of the SPR, was corroborated in the same gel with the band shift observed after adding streptavidin to the nanoparticles RGD-DNA nanoparticles.

Studying the binding affinity of the RGD-decorated DNA structures (RGD-DNA) to the αvβ3 integrin at the protein level using SPR:

To this point, it had been achieved RGD-DNA origami nanoparticles that were able to bind streptavidin. This was also confirmed with SPR. After functionalization of the gold sensor with streptavidin, the nanoparticles were injected and binding was observed with unbinding signal that remain stable after injection indicating stable binding on the surface (see **Figure 16 a)**. Having this platform allowed us to study binding affinity of the RGD-decorated

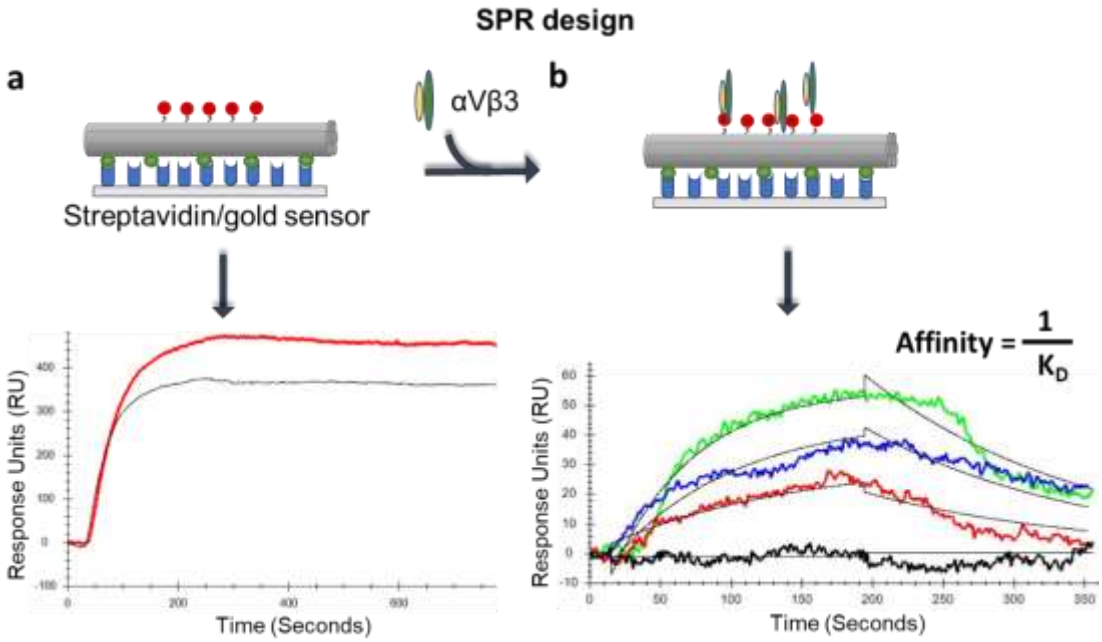

Figure 16. SPR experimental design and results. **a.** RGD-DNA NP immobilization. **b.** integrin αvβ3 binding curves

DNA structures (RGD-DNA) to the αvβ3 integrin. This was done at the protein level using the SPR technique as explained in page 29 of the methods. Briefly, the DNA-NP-RGD were immobilized on to the SPR sensor surface using streptavidin/biotin conjugation. Then, αvβ3 in a broad range of concentrations (from 0.5 nM to 53 nM) were injected to obtain the binding curves and kinetics of the interaction, and more specifically the K_D. An illustration of this along with an example of SPR results is given in **Figure 16 b**. Free RGD peptide was used as a positive control and DNA origami structures without RGD were the negative control or reference to account for non-specific binding. The binding affinity or strength of binding of RGD to αvβ3 integrin has already been measured with the SPR technique and has typically been reported by the equilibrium dissociation constant,

also known as K_D [62], [66]. In general, the value of K_D reported for RGD binding to αvβ3 varies between $2.4x10^{-9}$ M [66] and $1.3x10^{-6}$ M [62] depending on the experimental design and device used. In our case, the value of K_D measured for freely arranged RGD peptide was estimated at $4.3x10^{-8}$ M (**Figure 17**), which falls between the values reported in the literature for the same molecule.

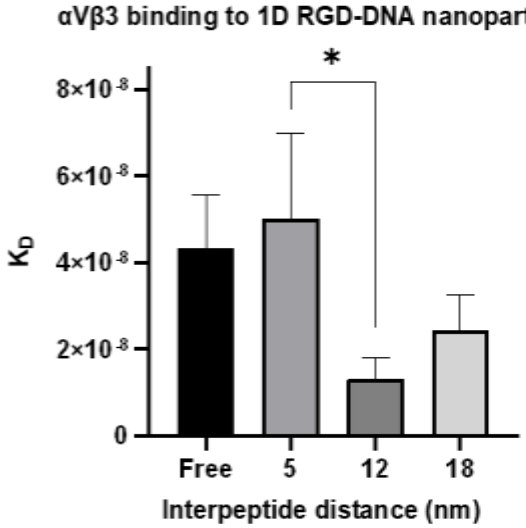

Interpeptide distance (nm)	KD
Free	4.3x10-8M
5	5.1x10-8M
12	1.3x10-8M
18	2.4x10-8M

Figure 17. Dissociation constant of freely arranged RGD and one-dimensionally arranged RGD on DNA nanoparticles to αvβ3 integrin at the molecular level .

Similarly, to test the possible role of one-dimensional nanoscale organization of RGD peptide on αvβ3 integrin binding, we used one dimensional DNA nanoparticles presenting five RGD peptide molecules equally distanced on the surface (see illustrations on **Figure 13**) and determined the values of K_D. **Figure 17** shows these values for freely arranged RGD, and 1D RGD-DNA nanoparticles with interpeptide distance of 5 nm, 12 nm and 18

nm. The rationale behind the chosen interpeptide distances was to be above, close and bellow the size of the αvβ3 integrin's head, that is reported to be between 8 nm and 12 nm [37].

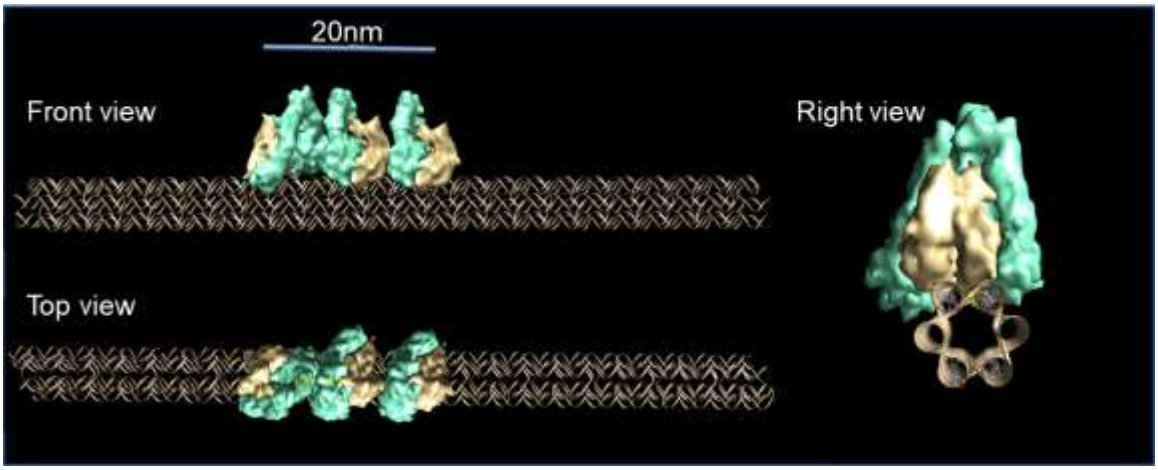

Figure 18. Model of the αvβ3 protein interacting with the 5nm inter-peptide 1D RGD-DNA.

Notably, no significant difference in K_D was observed between the free RGD ($4.3x10^{-8}$ M) and the RGD presented in one dimension at 5nm ($5.1x10^{-8}$ M) interpeptide distance, but a fivefold significant higher affinity (lower K_D) was observed at 12 nm interpeptide distance ($1.3x10^{-8}$ M). Additionally, a graphic model of the αvβ3 protein interacting with the 5 nm inter-peptide 1D RGD-DNA was recreated with the software Chimera, where we can see that only 3 out of five RGD molecules are accessible to the integrin (**Figure 18**). These results maybe indicating some degree of molecular crowding happening at interpeptide distances smaller than the head of the integrin, explaining the higher K_D value at smaller

interpeptide distance. However, at 18 nm the affinity was slightly lower ($1.3x10^{-8}$ M) than it was at 12 nm, but no significant difference was noted. Interestingly, similar results were observed by Veneziano et al. while using 1D DNA origami to explore the impact of antigen spacing on B-cell activation. They observed increasing activation of the cell up to 28 nm inter-antigen spacing, but a slight decrease or no change was observed at higher inter-antigen spacing [6].

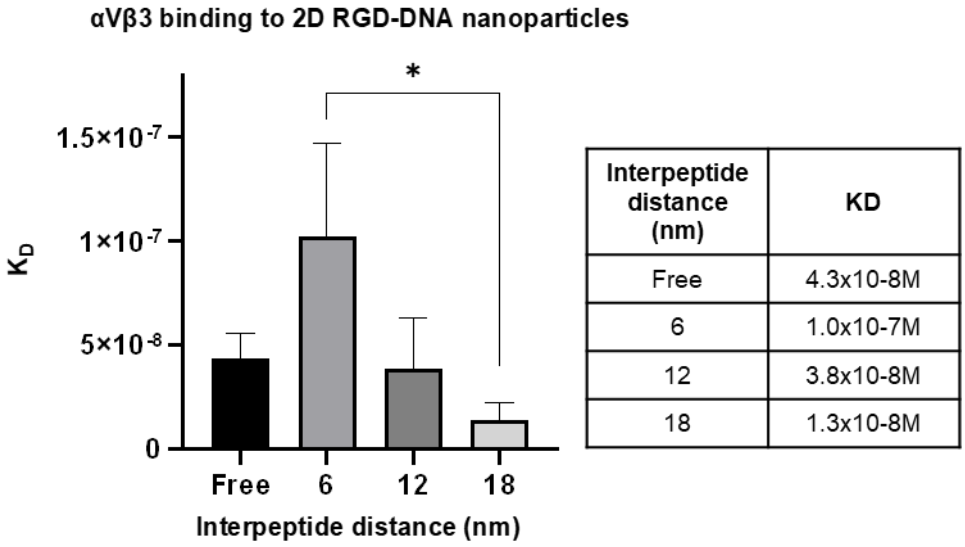

Interpeptide distance (nm)	KD
Free	4.3x10-8M
6	1.0x10-7M
12	3.8x10-8M
18	1.3x10-8M

Figure 19. Dissociation constant of freely arranged RGD and two-dimensionally arranged RGD on DNA nanoparticles to aVB3 integrin at the molecular level

The linear arrangement of peptide is useful to help elucidate the minimum peptide distance that maximizes the binding, but for many applications, 2D and even 3D arrangements of peptides are needed. Therefore, to test the potential role of two-dimensional nanoscale

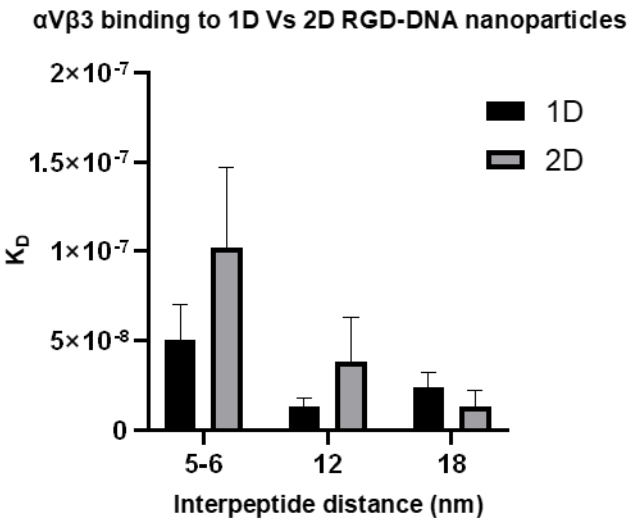

Interpeptide distance (nm)	Mean interpeptide distance(nm)	
	1D RGD-DNA	2D RGD-DNA
5-6	10	8
12	**24**	16
18	36	**24**

Figure 20. Dissociation constant of freely arranged RGD, one-dimensional and two-dimensional organizations of RGD on DNA nanoparticles to aVB3 integrin at the molecular level

organization of RGD peptide on αvβ3 integrin binding, we used pentagonal bipyramid DNA nanoparticles presenting 5 RGD peptide molecules equally distanced in a quasi-plane (see illustration of this in **Figure 13**) and determined the values of K_D from their binding curves in the SPR. The values of K_D obtained for these nanoparticles and the free RGD are shown in **Figure 19**, where it is clear a decreasing trend on the K_D as the inter-peptide distance increases. Significant difference in binding affinity to αvβ3 integrin was found between the 2D RGD-DNA nanoparticles with 6 nm interpeptide distance ($1.0x10^{-7}$ M) and 18 nm inter-peptide distance ($1.3x10^{-8}$ M), with a ten-fold higher affinity at 18 nm. The remarkably low affinity observed for the 2D pentagonal arrangement of RGD at 6 nm inter-peptide (even lower than that of the linear arrangement at 5 nm spacing) further confirms our proposition of molecular crowding affecting the interaction peptide-protein at distances smaller than the size of the protein head. Based on this results, we believe it is also crucial to consider the overall inter-peptide distance when comparing 1D to 2D peptide

presentations, as this is different for a linear and a pentagonal arrangement (see table of mean peptide distance in **Figure 20**). In fact, as indicated in **Figure 20**, the highest binding affinity of RGD-DNA nanoparticles was obtained with the 1D arrangement with inter-peptide distance of 12 nm and the 2D arrangement with 18 nm, which have in common an overall peptide distance of 24nm.

IV. Conclusions:

DNA nanoparticles presenting five RGD peptides (DNA-NP-RGD) in 1D and 2D with various inter-peptide spacing were investigated. The impact of linear peptide spacing on peptide-specific αvβ3 integrin binding was characterized and a 12 nm critical minimum needed distance for strong binding affinity was identified. Pentavalent 2D spatial arrangements of RGD were also evaluated for comparison with linear presentations of RGD to investigate the role of spatial presentation on αvβ3 integrin binding. A peptide spacing dependent trend was identified with maximum affinity at 18nm. Additionally, mean peptide distance was found as a common factor that can have an impact on RGD-αvβ3 integrin binding. This work shows promising results for the use and optimization of integrin-targeted DNA nanoparticle delivery. However, further work is required to better understand the factors affecting such binding interactions. For instance, more binding affinity measurement points for RGD linear arrangements with spacings between 5nm and 12nm and even higher than 18 nm are required to identify a trend or a better correlation. Similarly, for 2D arrangements, spacings higher than 18 nm would give us an inside to if there is a maximum distance at which the binding affinity is optimized.

V. Limitations and future work:

As mentioned before, greater understanding of the role of nanoscale organization can be achieved by evaluating more interpeptide distances and arrangements. Also, the role of stoichiometry in RGD-αvβ3 integrin binding interaction can be studied by comparing monovalent, bivalent, trivalent, etcetera RGD-DNA nanoparticles.

The structures that presented higher binding affinity for the αvβ3 integrin can be folded with the fluorescent DNA scaffold to evaluate membrane binding at the cellular level. PC3 is a prostate cancer cell line that highly expresses the αvβ3 integrin [67, p. 3], [68]. Then, it can be used to study the previous mentioned phenomena at the cellular level. Cells could be treated with these nanoparticles and studied by flow cytometry and fluorescence microscopy to quantify the binding efficiency. Specific membrane marker could be used to determine the fraction bound by precisely delimiting the cell membrane and the cytosol.

Not having control over the distance between the origami structures on SPR sensor surface was a limiting factor in this work. To overcome this, we used low concentrations of nanoparticles to produced undersaturated SPR surfaces, we assumed the nanostructures were far apart from each other. To solve this problem, it would be beneficial to use a technique such as soft lithography to be able to arrange the nanostructures on the sensor surface in highly defined patterns and distances [39].

Although, buffers containing Mg^{2+} ions stabilize the negative charge of the DNA origami, there is no measurement of the effect of DNA as the platform for this study. However, this limitation could be overcome by the integration of peptide nucleic acids, or PNA, in the DNA origami structures to reduce their overall negative charge [69].

Other projects and accomplishments

- Co-First authored “Synthesis of DNA Origami Scaffolds: Current and Emerging Strategies” published in the journal Molecules on July 2020
- Co-authored “Nano-bioink solutions for cardiac tissue bioprinting” published in Nanomedicine for Ischemic Cardiomyopathy on May2020
- Contributed to a research project carried by Dr. Igor Medintz at the U.S. Naval Research Laboratory (NRL) by synthesizing custom ssDNA scaffolds for DNA origami synthesis
- Participated in a research project on enhancement of computerized tomography (CT) scan carried by Dr. Vahid Serpooshan at the Georgia Institute of Technology, Emory School of Medicine with the production of Gadolinium -encapsulated liposomal suspensions.
- Founding member and secretary of the Graduate Association for Bioengineering Students (GABS) 2019-2020.

References

[1] B. Alberts, *Molecular Biology of the Cell*. Garland Science, 2017.

[2] S. L. Bellis, "Advantages of RGD peptides for directing cell association with biomaterials," *Biomaterials*, vol. 32, no. 18, pp. 4205–4210, Jun. 2011, doi: 10.1016/j.biomaterials.2011.02.029.

[3] Z. Li, B. Cao, X. Wang, K. Ye, S. Li, and J. Ding, "Effects of RGD nanospacing on chondrogenic differentiation of mesenchymal stem cells," *J. Mater. Chem. B*, vol. 3, no. 26, pp. 5197–5209, Jun. 2015, doi: 10.1039/C5TB00455A.

[4] A. Shaw *et al.*, "Spatial control of membrane receptor function using ligand nanocalipers," *Nature Methods*, vol. 11, no. 8, pp. 841–846, Aug. 2014, doi: 10.1038/nmeth.3025.

[5] A. Shaw *et al.*, "Binding to nanopatterned antigens is dominated by the spatial tolerance of antibodies," *Nature Nanotechnology*, vol. 14, no. 2, p. 184, Feb. 2019, doi: 10.1038/s41565-018-0336-3.

[6] R. Veneziano *et al.*, "Role of nanoscale antigen organization on B-cell activation probed using DNA origami," *Nature Nanotechnology*, vol. 15, no. 8, Art. no. 8, Aug. 2020, doi: 10.1038/s41565-020-0719-0.

[7] B. A. R. Williams, K. Lund, Y. Liu, H. Yan, and J. C. Chaput, "Self-Assembled Peptide Nanoarrays: An Approach to Studying Protein–Protein Interactions," *Angewandte Chemie International Edition*, vol. 46, no. 17, pp. 3051–3054, 2007, doi: 10.1002/anie.200603919.

[8] A. Rajendran, M. Endo, and H. Sugiyama, "Single-Molecule Analysis Using DNA Origami," *Angewandte Chemie International Edition*, vol. 51, no. 4, pp. 874–890, 2012, doi: 10.1002/anie.201102113.

[9] N. C. Seeman and H. F. Sleiman, "DNA nanotechnology," *Nat Rev Mater*, vol. 3, no. 1, pp. 1–23, Nov. 2017, doi: 10.1038/natrevmats.2017.68.

[10] P. W. K. Rothemund, "Folding DNA to create nanoscale shapes and patterns," *Nature*, vol. 440, no. 7082, pp. 297–302, Mar. 2006, doi: 10.1038/nature04586.

[11] R. Veneziano *et al.*, "Designer nanoscale DNA assemblies programmed from the top down," *Science*, vol. 352, no. 6293, pp. 1534–1534, Jun. 2016, doi: 10.1126/science.aaf4388.

[12] X. Liu, Y. Liu, and H. Yan, "Functionalized DNA Nanostructures for Nanomedicine," *Israel Journal of Chemistry*, vol. 53, no. 8, pp. 555–566, 2013, doi: 10.1002/ijch.201300002.

[13] C. R. Calladine, H. Drew, B. Luisi, and A. Travers, *Understanding DNA: The Molecule and How It Works*. Saint Louis, UNITED KINGDOM: Elsevier Science & Technology, 2004.
[14] N. C. Seeman, "Nucleic acid junctions and lattices," *Journal of Theoretical Biology*, vol. 99, no. 2, pp. 237–247, Nov. 1982, doi: 10.1016/0022-5193(82)90002-9.
[15] B. Saccà *et al.*, "Orthogonal Protein Decoration of DNA Origami," *Angewandte Chemie*, vol. 122, no. 49, pp. 9568–9573, 2010, doi: 10.1002/ange.201005931.
[16] B. Saccà and C. M. Niemeyer, "Functionalization of DNA nanostructures with proteins," *Chemical Society Reviews*, vol. 40, no. 12, pp. 5910–5921, 2011, doi: 10.1039/C1CS15212B.
[17] C. Timm and C. M. Niemeyer, "Assembly and Purification of Enzyme-Functionalized DNA Origami Structures," *Angewandte Chemie International Edition*, vol. 54, no. 23, pp. 6745–6750, 2015, doi: 10.1002/anie.201500175.
[18] J. Chao, H. Liu, S. Su, L. Wang, W. Huang, and C. Fan, "Structural DNA Nanotechnology for Intelligent Drug Delivery," *Small*, vol. 10, no. 22, pp. 4626–4635, Nov. 2014, doi: 10.1002/smll.201401309.
[19] M. Tintoré, I. Gállego, B. Manning, R. Eritja, and C. Fàbrega, "DNA Origami as a DNA Repair Nanosensor at the Single-Molecule Level," *Angewandte Chemie International Edition*, vol. 52, no. 30, pp. 7747–7750, 2013, doi: 10.1002/anie.201301293.
[20] Q. Zhang *et al.*, "DNA Origami as an In Vivo Drug Delivery Vehicle for Cancer Therapy," *ACS Nano*, vol. 8, no. 7, pp. 6633–6643, Jul. 2014, doi: 10.1021/nn502058j.
[21] Y.-X. Zhao, A. Shaw, X. Zeng, E. Benson, A. M. Nyström, and B. Högberg, "DNA Origami Delivery System for Cancer Therapy with Tunable Release Properties," *ACS Nano*, vol. 6, no. 10, pp. 8684–8691, Oct. 2012, doi: 10.1021/nn3022662.
[22] J. Nangreave, D. Han, Y. Liu, and H. Yan, "DNA origami: a history and current perspective," *Current Opinion in Chemical Biology*, vol. 14, no. 5, pp. 608–615, Oct. 2010, doi: 10.1016/J.CBPA.2010.06.182.
[23] T. J. Fu and N. C. Seeman, "DNA double-crossover molecules," *Biochemistry*, vol. 32, no. 13, pp. 3211–3220, Apr. 1993, doi: 10.1021/bi00064a003.
[24] A. R. Chandrasekaran, "DNA origami and biotechnology applications: a perspective," *Journal of Chemical Technology & Biotechnology*, vol. 91, no. 4, pp. 843–846, 2016, doi: 10.1002/jctb.4826.
[25] Y. Ke, S. Lindsay, Y. Chang, Y. Liu, and H. Yan, "Self-Assembled Water-Soluble Nucleic Acid Probe Tiles for Label-Free RNA Hybridization Assays," *Science*, vol. 319, no. 5860, pp. 180–183, Jan. 2008, doi: 10.1126/science.1150082.
[26] S. Rinker, Y. Ke, Y. Liu, R. Chhabra, and H. Yan, "Self-assembled DNA nanostructures for distance-dependent multivalent ligand–protein binding," *Nature Nanotech*, vol. 3, no. 7, pp. 418–422, Jul. 2008, doi: 10.1038/nnano.2008.164.
[27] H. Kubas *et al.*, "Multivalent cyclic RGD ligands: influence of linker lengths on receptor binding," *Nuclear Medicine and Biology*, vol. 37, no. 8, pp. 885–891, Nov. 2010, doi: 10.1016/j.nucmedbio.2010.06.005.

[28] C. V. Carman and T. A. Springer, “Integrin avidity regulation: are changes in affinity and conformation underemphasized?,” *Current Opinion in Cell Biology*, vol. 15, no. 5, pp. 547–556, Oct. 2003, doi: 10.1016/j.ceb.2003.08.003.
[29] J. Hedhli *et al.*, “Synthesis, Chemical Characterization and Multiscale Biological Evaluation of a Dimeric-cRGD Peptide for Targeted Imaging of α V β 3 Integrin Activity,” *Scientific Reports*, vol. 7, no. 1, p. 3185, Jun. 2017, doi: 10.1038/s41598-017-03224-8.
[30] E. Garanger, D. Boturyn, J.-L. Coll, M.-C. Favrot, and P. Dumy, “Multivalent RGD synthetic peptides as potent αVβ3 integrin ligands,” *Org. Biomol. Chem.*, vol. 4, no. 10, pp. 1958–1965, May 2006, doi: 10.1039/B517706E.
[31] X. Montet, M. Funovics, K. Montet-Abou, R. Weissleder, and L. Josephson, “Multivalent Effects of RGD Peptides Obtained by Nanoparticle Display,” *J. Med. Chem.*, vol. 49, no. 20, pp. 6087–6093, Oct. 2006, doi: 10.1021/jm060515m.
[32] L. Y. Koo, D. J. Irvine, A. M. Mayes, D. A. Lauffenburger, and L. G. Griffith, “Co-regulation of cell adhesion by nanoscale RGD organization and mechanical stimulus,” *Journal of Cell Science*, vol. 115, no. 7, pp. 1423–1433, Apr. 2002.
[33] G. Maheshwari, G. Brown, D. A. Lauffenburger, A. Wells, and L. G. Griffith, “Cell adhesion and motility depend on nanoscale RGD clustering,” *J Cell Sci*, vol. 113, no. 10, pp. 1677–1686, May 2000.
[34] F. Danhier, A. Le Breton, and V. Préat, “RGD-Based Strategies To Target Alpha(v) Beta(3) Integrin in Cancer Therapy and Diagnosis,” *Mol. Pharmaceutics*, vol. 9, no. 11, pp. 2961–2973, Nov. 2012, doi: 10.1021/mp3002733.
[35] E. Jo *et al.*, “Peptide ligand-mediated endocytosis of nanoparticles to cancer cells: Cell receptor-binding- versus cell membrane-penetrating peptides,” *Biotechnology and Bioengineering*, vol. 115, no. 6, pp. 1437–1449, 2018, doi: 10.1002/bit.26575.
[36] J. Huang *et al.*, “Impact of Order and Disorder in RGD Nanopatterns on Cell Adhesion,” *Nano Lett.*, vol. 9, no. 3, pp. 1111–1116, Mar. 2009, doi: 10.1021/nl803548b.
[37] M. Schvartzman *et al.*, “Nanolithographic Control of the Spatial Organization of Cellular Adhesion Receptors at the Single-Molecule Level,” *Nano Lett.*, vol. 11, no. 3, pp. 1306–1312, Mar. 2011, doi: 10.1021/nl104378f.
[38] J. Li, Y. Chen, N. Kawazoe, and G. Chen, “Ligand density-dependent influence of arginine–glycine–aspartate functionalized gold nanoparticles on osteogenic and adipogenic differentiation of mesenchymal stem cells,” *Nano Res.*, vol. 11, no. 3, pp. 1247–1261, Mar. 2018, doi: 10.1007/s12274-017-1738-5.
[39] W. Hawkes *et al.*, “Probing the nanoscale organisation and multivalency of cell surface receptors: DNA origami nanoarrays for cellular studies with single-molecule control,” *Faraday Discuss.*, Mar. 2019, doi: 10.1039/C9FD00023B.
[40] R. Veneziano, T. R. Shepherd, S. Ratanalert, L. Bellou, C. Tao, and M. Bathe, “In vitro synthesis of gene-length single-stranded DNA,” *Scientific Reports*, vol. 8, no. 1, pp. 1–7, Apr. 2018, doi: 10.1038/s41598-018-24677-5.

[41] P. Charoenphol and H. Bermudez, “Design and application of multifunctional DNA nanocarriers for therapeutic delivery,” *Acta Biomaterialia*, vol. 10, no. 4, pp. 1683–1691, Apr. 2014, doi: 10.1016/j.actbio.2013.07.021.
[42] H. Ijäs, I. Hakaste, B. Shen, M. A. Kostiainen, and V. Linko, “Reconfigurable DNA Origami Nanocapsule for pH-Controlled Encapsulation and Display of Cargo,” *ACS Nano*, vol. 13, no. 5, pp. 5959–5967, May 2019, doi: 10.1021/acsnano.9b01857.
[43] J. Fu and H. Yan, “Controlled drug release by a nanorobot,” *Nature Biotechnology*, vol. 30, no. 5, Art. no. 5, May 2012, doi: 10.1038/nbt.2206.
[44] P. Wang, T. A. Meyer, V. Pan, P. K. Dutta, and Y. Ke, “The Beauty and Utility of DNA Origami,” *Chem*, vol. 2, no. 3, pp. 359–382, Mar. 2017, doi: 10.1016/j.chempr.2017.02.009.
[45] A. R. Chandrasekaran, M. Pushpanathan, and K. Halvorsen, “Evolution of DNA origami scaffolds,” *Materials Letters*, vol. 170, pp. 221–224, May 2016, doi: 10.1016/j.matlet.2016.01.161.
[46] F. A. S. Engelhardt *et al.*, “Custom-Size, Functional, and Durable DNA Origami with Design-Specific Scaffolds,” *ACS Nano*, vol. 13, no. 5, pp. 5015–5027, May 2019, doi: 10.1021/acsnano.9b01025.
[47] J. Bush, S. Singh, M. Vargas, E. Oktay, C.-H. Hu, and R. Veneziano, “Synthesis of DNA Origami Scaffolds: Current and Emerging Strategies,” *Molecules*, vol. 25, no. 15, Art. no. 15, Jan. 2020, doi: 10.3390/molecules25153386.
[48] M. Hao, J. Qiao, and H. Qi, “Current and Emerging Methods for the Synthesis of Single-Stranded DNA,” *Genes*, vol. 11, no. 2, Art. no. 2, Feb. 2020, doi: 10.3390/genes11020116.
[49] E. Pound, J. R. Ashton, H. A. Becerril, and A. T. Woolley, “Polymerase Chain Reaction Based Scaffold Preparation for the Production of Thin, Branched DNA Origami Nanostructures of Arbitrary Sizes,” *Nano Lett.*, vol. 9, no. 12, pp. 4302–4305, Dec. 2009, doi: 10.1021/nl902535q.
[50] T.-C. Kuo, “Streamlined method for purifying single-stranded DNA from PCR products for frequent or high-throughput needs,” *BioTechniques*, vol. 38, no. 5, pp. 700–702, May 2005, doi: 10.2144/05385BM04.
[51] M. Yuce, H. Kurt, and H. Budak, “Characterization of a dual biotin tag for improved single stranded DNA production,” *Anal. Methods*, vol. 6, no. 2, pp. 548–557, Dec. 2013, doi: 10.1039/C3AY41899E.
[52] H. Zhang, J. Chao, D. Pan, H. Liu, Q. Huang, and C. Fan, “Folding super-sized DNA origami with scaffold strands from long-range PCR,” *Chem. Commun.*, vol. 48, no. 51, pp. 6405–6407, May 2012, doi: 10.1039/C2CC32204H.
[53] D. Han *et al.*, “Single-stranded DNA and RNA origami,” *Science*, vol. 358, no. 6369, Dec. 2017, doi: 10.1126/science.aao2648.
[54] M. Avci-Adali, A. Paul, N. Wilhelm, G. Ziemer, and H. P. Wendel, “Upgrading SELEX Technology by Using Lambda Exonuclease Digestion for Single-Stranded DNA Generation,” *Molecules*, vol. 15, no. 1, pp. 1–11, Dec. 2009, doi: 10.3390/molecules15010001.

[55] R. G. Higuchi and H. Ochman, “Production of single-stranded DNA templates by exonuclease digestion following the polymerase chain reaction,” *Nucleic Acids Res*, vol. 17, no. 14, pp. 5865–5865, Jul. 1989, doi: 10.1093/nar/17.14.5865.
[56] V. E. Shershov *et al.*, “Comparative Study of Novel Fluorescent Cyanine Nucleotides: Hybridization Analysis of Labeled PCR Products Using a Biochip,” *J Fluoresc*, vol. 27, no. 6, pp. 2001–2016, Nov. 2017, doi: 10.1007/s10895-017-2139-6.
[57] E. Eremeeva, M. Abramov, L. Margamuljana, and P. Herdewijn, “Base-Modified Nucleic Acids as a Powerful Tool for Synthetic Biology and Biotechnology,” *Chemistry – A European Journal*, vol. 23, no. 40, pp. 9560–9576, Jul. 2017, doi: 10.1002/chem.201700679.
[58] E. Eremeeva and P. Herdewijn, “PCR Amplification of Base-Modified DNA,” *Current Protocols in Chemical Biology*, vol. 10, no. 1, pp. 18–48, Mar. 2018, doi: 10.1002/cpch.33.
[59] T. Tasara *et al.*, “Incorporation of reporter molecule-labeled nucleotides by DNA polymerases. II. High-density labeling of natural DNA,” *Nucleic Acids Res*, vol. 31, no. 10, pp. 2636–2646, May 2003, doi: 10.1093/nar/gkg371.
[60] R. Fregel, A. González, and V. M. Cabrera, “Improved ethanol precipitation of DNA,” *ELECTROPHORESIS*, vol. 31, no. 8, pp. 1350–1352, 2010, doi: 10.1002/elps.200900721.
[61] G. Cosa, K.-S. Focsaneanu, J. R. N. McLean, J. P. McNamee, and J. C. Scaiano, “Photophysical Properties of Fluorescent DNA-dyes Bound to Single- and Double-stranded DNA in Aqueous Buffered Solution¶,” *Photochemistry and Photobiology*, vol. 73, no. 6, pp. 585–599, 2001, doi: 10.1562/0031-8655(2001)0730585PPOFDD2.0.CO2.
[62] Y. Liu, Y. Pan, and Y. Xu, “Binding Investigation of Integrin αvβ3 With Its Inhibitors by SPR Technology and Molecular Docking Simulation,” *J Biomol Screen*, vol. 15, no. 2, pp. 131–137, Feb. 2010, doi: 10.1177/1087057109356207.
[63] E.-K. Sinner *et al.*, “Incorporation of integrins into artificial planar lipid membranes: characterization by plasmon-enhanced fluorescence spectroscopy,” *Analytical Biochemistry*, vol. 333, no. 2, pp. 216–224, Oct. 2004, doi: 10.1016/j.ab.2004.05.022.
[64] D. Bernhagen *et al.*, “Bicyclic RGD Peptides with Exquisite Selectivity for the Integrin αvβ3 Receptor Using a ‘Random Design’ Approach,” *ACS Comb. Sci.*, vol. 21, no. 3, pp. 198–206, Mar. 2019, doi: 10.1021/acscombsci.8b00144.
[65] J.-F. Lutz, “Copper-Free Azide–Alkyne Cycloadditions: New Insights and Perspectives,” *Angewandte Chemie International Edition*, vol. 47, no. 12, pp. 2182–2184, 2008, doi: 10.1002/anie.200705365.
[66] J. R. Klim *et al.*, “Small Molecule-Modified Surfaces Engage Cells Through the αvβ3 Integrin,” *ACS Chem Biol*, vol. 7, no. 3, pp. 518–525, Mar. 2012, doi: 10.1021/cb2004725.
[67] S. Tai *et al.*, “PC3 Is a Cell Line Characteristic of Prostatic Small Cell Carcinoma,” *Prostate*, vol. 71, no. 15, pp. 1668–1679, Nov. 2011, doi: 10.1002/pros.21383.

[68] S. Dall'Angelo *et al.*, "Efficient bioconjugation of 5-fluoro-5-deoxy-ribose (FDR) to RGD peptides for positron emission tomography (PET) imaging of αvβ3 integrin receptor," *Org. Biomol. Chem.*, vol. 11, no. 27, pp. 4551–4558, Jun. 2013, doi: 10.1039/C3OB40550H.
[69] S. Shakeel, S. Karim, and A. Ali, "Peptide nucleic acid (PNA) — a review," *Journal of Chemical Technology & Biotechnology*, vol. 81, no. 6, pp. 892–899, 2006, doi: 10.1002/jctb.1505.
[70] P. P. Rath, G. Anand, and S. Agarwal, "Surface Plasmon Resonance Analysis of the Protein-protein Binding Specificity Using Autolab ESPIRIT," *Bio-protocol*, vol. 10, no. 4, pp. e3519–e3519, Feb. 2020.

Biography

Merlyn Vargas studied chemistry at Universidad de Antioquia (Colombia) and received her BS research with honors on: "*Synthesis of metallic nanoparticles supported in carbon nanotubes and coated with graphene layers*". During her research internship at the Webster nanomedicine lab at Northeastern University in Boston, she developed profound interest in the field of biotechnology. Finally, in 2019 she joined Dr. Remi Veneziano's laboratory to research on DNA nanotechnology for applications in materials science and nanomedicine.